Materials Today Energy 32 (2023) 101232

Contents lists available at ScienceDirect

Materials Today Energy

journal homepage: www.journals.elsevier.com/materials-today-energy/

Vanadium-based cathode materials for rechargeable magnesium batteries

X. Zhang, D. Li, Q. Ruan, L. Liu, B. Wang, F. Xiong***, C. Huang**, P.K. Chu*

Department of Physics, Department of Materials Science and Engineering, and Department of Biomedical Engineering, City University of Hong Kong, Tat Chee Avenue, Kowloon, Hong Kong, China

ARTICLE INFO

Article history:
Received 12 October 2022
Received in revised form
1 December 2022
Accepted 17 December 2022
Available online 23 December 2022

Keywords:
Rechargeable magnesium battery
Vanadium oxide
Vanadate
Vanadium chalcogenide
Vanadium-based phosphate

ABSTRACT

Rechargeable magnesium batteries (RMBs) are promising candidates for large-scale energy storage due to the low cost, abundant reserve, high volumetric capacity, and low redox potential of Mg anodes. Since the high theoretical capacity and energy density originate from the rich valence states of vanadium (from +2 to +5) and distortion of V–O polyhedrons, vanadium-based cathode materials are very attractive for RMBs. This paper provides a comprehensive overview of vanadium-based cathode materials for RMBs including vanadium oxides, vanadates, vanadium chalcogenides, and vanadium-based phosphates. The structure, electrochemical properties, optimization strategies, structure–performance relationship, and reaction mechanisms of various vanadium-based cathode materials are described. The challenges, prospective, and future research directions of vanadium-based electrode materials are discussed.

1. Introduction

Green and renewable energy sources such as wind and solar energy are vital to sustainable development [1,2]. However, since their availability depend on nature, they are not as reliable as traditional sources such as coal and gas in supplying continuous electricity to the power grid. One solution is to build smart grids based on large-scale energy storage systems (LSESSs) to store the electricity generated by renewable energy sources [3–5]. Since application of lithium-ion batteries (LIBs) to LSESSs is hindered by the high price and limited natural lithium reserve, it is imperative to identify suitable alternatives [6,7]. Because of the low cost and abundant reserve of magnesium, rechargeable magnesium batteries (RMBs) have garnered increasing interest as alternatives to LIBs for LSESSs [8–10]. Moreover, Mg anodes have a high volumetric capacity (3,833 mAh/cm^3) and low redox potential (−2.37 V vs. standard hydrogen electrode) [9–13].

The radius of Mg ions (0.72 Å) is similar to that of Li ions (0.76 Å), but intercalation of Mg ions is more difficult in the same host due to the charge difference [11,14]. The large charge/radius ratio of divalent Mg ions results in strong electrostatic interactions between Mg ions and cathode materials making intercalation and diffusion sluggish [9–12,15]. As a result, most cathode materials for RMBs exhibit a small degree of magnesiation, large voltage hysteresis, and low rates [11,16,17]. Therefore, it is important to identify and develop new and high-performance cathode materials for RMBs.

Different materials have hitherto been explored as cathode materials for RMBs, for example, transition metal chalcogenides [18–22], transition metal oxides [23–26], polyanionic compounds [27–29], organic materials [30,31], and so on [32,33]. In particular, vanadium-based materials have attracted much attention due to the high theoretical capacity and energy density stemming from the rich valence states of vanadium (+2 to +5) [34,35]. Many vanadium-based materials have the layered structure or open framework, which is favorable to intercalation and diffusion of Mg ions. Furthermore, flexible distortion of V–O polyhedrons facilitates accommodation of intercalated Mg ions. Vanadium-based cathode materials suitable for RMBs are primarily vanadium oxides, vanadates, vanadium chalcogenides, and vanadium-based phosphates. In this review, vanadium-based cathode materials are reviewed. In addition to the electrochemical properties, the reaction mechanisms, optimization strategies, and structure-

* Corresponding author.
** Corresponding author.
*** Corresponding author.
E-mail addresses: fxiong@cityu.edu.hk (F. Xiong), chuang46-c@my.cityu.edu.hk (C. Huang), paul.chu@cityu.edu.hk (P.K. Chu).

https://doi.org/10.1016/j.mtener.2022.101232
2468-6069/

properties relationship are described. Finally, the challenges and outlook of vanadium-based electrode materials are discussed.

2. Vanadium oxides

Vanadium exists in different valence states in oxides including V_2O_5, $V_2O_5 \cdot nH_2O$, VO_2, $V_3O_7 \cdot H_2O$ ($H_2V_3O_8$), V_6O_{13}, and V_2O_3 (Fig. 1). The V−O polyhedrons in vanadium oxides can be square pyramids, octahedrons, or both, whereas M−O polyhedrons in other transition metal oxides are usually octahedrons. This shows the facile distortion nature of V−O polyhedrons. Some vanadium oxides such as V_2O_5 and VO_2 have multiple polymorphs and so the vanadium oxide family is quite large. Common vanadium oxides that have been studied as cathode materials for RMBs are described in this section.

2.1. V_2O_5

Orthorhombic V_2O_5 (α-V_2O_5) has the layered structure in which the layers consisting of alternating edge- and corner-sharing distorted VO_5 square pyramids are stacked along the c-axis with an interlayer spacing of 4.37 Å (Fig. 1a). Owing to the unique structure, orthorhombic V_2O_5 has attracted much attraction in the energy storage field as an intercalation host for different ions. Pereira-Ramos et al. have demonstrated that Mg ions can be intercalated electrochemically into orthorhombic V_2O_5 at 150 °C [36]. Yu and coworkers have also confirmed the electrochemical intercalation of Mg ions into orthorhombic V_2O_5 in solid-state RMBs composed of the metallic Mg anode, Mg-montmorillonite electrolyte and V_2O_5 cathode [37]. Gregory et al. have reported that 0.66 mol of Mg can be intercalated into 1 mol of V_2O_5 by chemical intercalation in the dibutylmagnesium/heptane solution at room temperature, corresponding to a high capacity of 194 mAh/g [38]. This value is consistent with the capacity determined electrochemically in the 1 M $Mg(ClO_4)_2$/tetrahydrofuran (THF) electrolyte. These early results demonstrate that V_2O_5 is a promising cathode in RMBs.

The water content in the electrolyte plays an important role in the electrochemical properties and reaction mechanism of V_2O_5. Novák et al. first reported that the water content in $Mg(ClO_4)_2$/acetonitrile (AN) electrolyte affects the magnesium storage capacity of V_2O_5 [39]. The V_2O_5 cathode shows a capacity of 170 mAh/g in 1 M $Mg(ClO_4)_2$/AN with 1 M H_2O and the capacity is higher than that in the dry 1 M $Mg(ClO_4)_2$/AN electrolyte (~25 mAh/g). However, the capacity of V_2O_5 in 1 M $Mg(ClO_4)_2$/AN with 1 M H_2O decays to ~50 mAh/g in 20 cycles. V_2O_5 also exhibits improved capacity in $Mg(ClO_4)_2$/propylene carbonate (PC) and magnesium bis(trifluoromethane sulfonyl)imide (Mg (TFSI)$_2$)/diglyme (G2) electrolytes containing the proper amount of water [40,41]. S-doped V_2O_5 and MnO_2/S-doped V_2O_5 reported by Inamoto et al. show high reversible capacities of 300 mAh/g and 420 mAh/g in the 0.3 M $Mg(ClO_4)_2$/PC electrolyte containing 1.8 M H_2O, respectively [42]. Unfortunately, water produces passive layers on Mg anodes consequently hindering reversible Mg plating/striping [40,41]. Meanwhile, the higher capacity of V_2O_5 in electrolytes containing water may be caused by intercalation of protons. Lim et al. have shown that the discharged product of α-V_2O_5 in 0.5 M $Mg(ClO_4)_2$/AN and 2.0 M H_2O is $Mg_{0.17}H_xV_2O_5$ ($0.66 \leq x \leq 1.16$), indicating that the capacity is mainly attributable to proton intercalation [43]. Solid-state nuclear magnetic resonance (NMR) also indicates that reversible proton insertion provides the main capacity of α-V_2O_5 in an electrolyte with a large water content [41]. In fact, proton intercalation consumes the electrolyte so that this system requires more electrolyte in practice compared to the “rock-chair” type RMBs, resulting in a decrease in the energy density. Therefore, the water content in the electrolyte used in the study needs to be characterized but has been ignored in many studies.

The reaction mechanism of α-V_2O_5 in RMBs with a dry electrolyte is not well understood. According to Verrelli et al., proton intercalation dominates the reaction of α-V_2O_5 even in an anhydrous electrolyte and the intercalation of Mg ions is negligible [44]. However, Mukherjee et al. have observed Mg intercalation in α-V_2O_5 by atomic-resolution transmission electron microscopy [45]. The co-existed α-V_2O_5 and ε-$Mg_{0.5}V_2O_5$ phases are observed from the discharged α-V_2O_5 and the observation is consistent with first-principles calculation by Ceder and co-workers [46]. Recently, Fu et al. have employed *in situ* synchrotron diffraction (Fig. 2a) and *in situ* X-ray absorption near-edge spectroscopy (XANES) to study the reaction mechanism of α-V_2O_5 cathodes in RMBs [47]. During discharging, α-V_2O_5 changes to an Mg-poor phase ($Mg_{0.14}V_2O_5$) *via* a solid solution process and then undergoes a two-phase transition

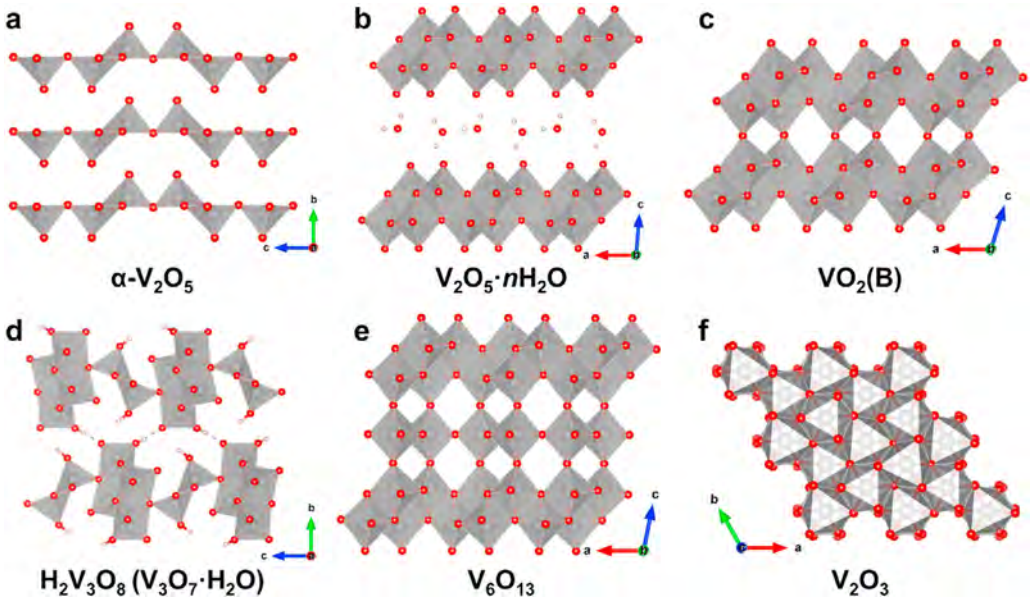

Fig. 1. Schematic illustration of the crystal structure of various vanadium oxides: (a) α-V_2O_5, (b) $V_2O_5 \cdot nH_2O$, (c) VO_2(B), (d) $H_2V_3O_8$ ($V_3O_7 \cdot H_2O$), (e) V_6O_{13}, and (f) V_2O_3.

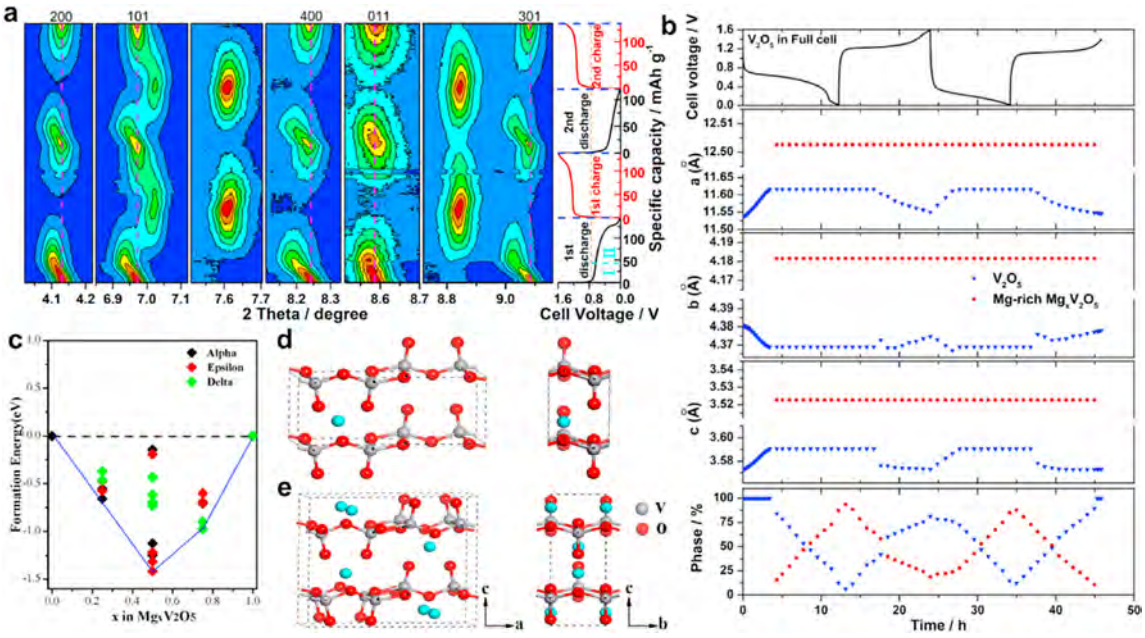

Fig. 2. Magnesium storage mechanism of α-V_2O_5. (a) *In situ* synchrotron diffraction patterns and (b) Structural parameters and phase ratios for the first two cycles of V_2O_5 [47]. (c) Formation energy of Mg intercalation in α-V_2O_5, ε-V_2O_5, and δ-V_2O_5 at different concentrations and crystal structures of (d) ε-V_2O_5 and (e) δ-V_2O_5 with intercalated metal ions (blue balls) [48].

between the Mg-poor phase and Mg-rich phase ($Mg_{0.6}V_2O_5$) (Fig. 2b). As the $Mg_{0.6}V_2O_5$ phase retains the basic structure of α-V_2O_5, it can be considered as the ε-$Mg_{0.6}V_2O_5$ phase that is similar to the ε-$Mg_{0.5}V_2O_5$ phase. On account of the limited capacity (144 mAh/g), the two-phase transition is not complete at the end of discharging. Moreover, XANES and X-ray photoelectron spectroscopy (XPS) demonstrate reduction of partial V^{5+} to V^{4+} during the discharging process. Xiao et al. have observed that α-V_2O_5 transforms to the ε-phase and then δ-phase as the concentration of intercalated Mg increases from 0 → 0.5 → 1 based on the first-principles calculation (Fig. 2d–f) [48]. Yoo et al. have suggested that the fully charged product (1 Mg per V_2O_5) of α-V_2O_5 at 110 °C is not δ-MgV_2O_5, but rather an unknown phase with a local electronic environment of Mg^{2+} similar to δ-MgV_2O_5 [49]. All in all, in spite of these earlier studies, the magnesium storage mechanism of α-V_2O_5, especially for high Mg intercalation concentration, is still not well understood.

Besides the water content, the effects of the solvent and anions in the electrolyte on magnesium storage of α-V_2O_5 have been investigated. Attias et al. have suggested that the TFSI anion reacts with the V_2O_5 electrode to form a surface film consisting mainly of MgF_2 to impede Mg intercalation [50]. 1, 2-dimethoxyethane (DME) in the $Mg(ClO_4)_2$/AN electrolyte mitigates charge transfer across the V_2O_5 and electrolyte interface because DME causes ACN-Mg^{2+} to be replaced by more stable solvated 3DME-Mg^{2+} [51]. So far there have few studies on the effects of solvents and anions on the magnesium storage characteristics of vanadium-based materials. The origin of the difference in the compatibility of vanadium oxides with different electrolytes remains unclear.

The strong electrostatic interactions between bivalent Mg^{2+} and lattice oxygen produce slow diffusion of Mg ions in α-V_2O_5 and this is one of the major reasons for the unsatisfactory magnesium storage properties. Nanostructures can increase the active surface area and reduce the diffusion distance to improve the electrochemical properties of α-V_2O_5. For example, Amatucci et al. have observed that α-V_2O_5 nanoparticles with diameters of 20–50 nm have a reversible capacity of 180 mAh/g at 7.6 mA/g in 0.5 M $Mg(ClO_4)_2$/PC [52]. Gershinsky et al. have fabricated V_2O_5 films with nanoscale thickness and particle size [23]. In the 0.5 M $Mg(ClO_4)_2$/AN electrolyte, the V_2O_5 thin film has an initial capacity of 180 mAh/g and it remains at 150 mAh/g after 36 cycles. Mukherjee et al. have prepared α-V_2O_5 nanospheres with a reversible capacity of ~190 mAh/g at 10 mA/g in 0.2 M $Mg(ClO_4)_2$/AN [53]. However, the capacity of V_2O_5 nanospheres drops to ~40 mAh/g when the current density is increased to 80 mA/g. In addition, nanostructured α-V_2O_5 has attractive magnesium storage capacity in electrolytes compatible with metallic Mg anodes. Xiao et al. have reported that V_2O_5 microflowers composed of 25 nm thick nanosheets show an initial capacity of 126.2 mAh/g at 50 mA/g in 0.25 M $Mg(AlCl_2EtBu)_2$/THF and it remains at 90.7 mAh/g after 80 cycles [54]. The graphene oxide (GO)/V_2O_5 composite reported by Du et al. has an initial capacity of 178 mAh/g in the 0.25 M $Mg(AlCl_2EtBu)_2$/THF and 140 mAh/g after 20 cycles [55]. Sheha et al. have also prepared V_2O_5/GO composites but the electrochemical properties are relatively poor due to the mismatched electrolyte [56].

A higher temperature enhances diffusion of Mg ions and improves the magnesium storage capacity of α-V_2O_5. Yoo et al. have evaluated the electrochemical characteristics of α-V_2O_5 in 0.5 M Mg $(TFSI)_2$/1-butyl-1-methylpyrrolidinium bis(trifluoromethyl sulfonyl)imide ($PY_{14}TFSI$) electrolyte at different temperature and found that the magnesium storage capacity increases from 16 mAh/g to 295 mAh/g when the temperature is raised from 25 °C to 110 °C [49]. At 110 °C and after cycling at 0.05C, the capacity of α-V_2O_5 is 150 mAh/g at 2 C and capacity retention is 76% after 50 cycles at C/5. After one conditioning cycle at 110 °C, the capacity of α-V_2O_5 at 25 °C increases to 96 mAh/g and remains stable for 20 cycles. Johnson et al. have prepared the V_2O_5–TiO_2 composite with an average crystallite diameter of 25 nm and observed an enhanced magnesium storage capacity of 310 mAh/g at 110 °C which is higher than that of V_2O_5 with an average crystallite diameter of 140 nm (230 mAh/g) [57]. However, the solvents in most RMBs electrolytes, including THF, DME, AN, and so forth, have a low boiling point

(<90 °C), rendering their not suitable at a high temperature. Meanwhile, the required high operating temperature also limits the range of applications.

Introduction of oxygen vacancies is an efficient way to boost the electrical conductivity and diffusion kinetics of metal oxides [6,61]. Wu et al. have fabricated honeycombed V_2O_5 with rich oxygen vacancies on a Ti foil (Ti−V_2O_{5-x}) (Fig. 3a and b) [58]. In the 0.5 M $Mg(ClO_4)_2$/AN electrolyte, Ti−V_2O_{5-x} shows magnesium storage capacities of 250 mAh/g at 100 mA/g with a discharge plateau at 2.1 V (*vs.* Mg^{2+}/Mg) (Fig. 3c) and 195.4 mAh/g after 400 cycles. At 500 mA/g, the capacity of Ti−V_2O_{5-x} is still 148 mAh/g, which is higher than that of Ti−V_2O_5 without rich oxygen vacancies (57.2 mAh/g). The enhanced conductivity and Mg diffusion kinetics are responsible for the better magnesium storage properties.

The interlayer regulation strategy has been employed to modify α-V_2O_5. Yang et al. have carried out *ab initio* investigation on V_2O_5 pre-intercalated with Li^+, Na^+, and Al^{3+} as cathode materials for RMBs and found that metal pre-intercalation improves the electrical conductivity of V_2O_5 and reduces the diffusion barrier of Mg ions [59]. Yao et al. have synthesized poly (3,4-ethylenedioxythiophene) (PEDOT) intercalated V_2O_5 (VOP) with an expanded interlayer spacing (9.86 Å) and in the 0.4 M $(PhMgCl)_2$−$AlCl_3$/THF (APC/THF) electrolyte containing the cetyltrimethylammonium bromide (CTAB) additive, VOP displays a reversible capacity of 288.7 mAh/g at 50 mA/g and rate capability of 110.7 mAh/g at 500 mA/g [62]. After 500 cycles at 500 mA/g, the capacity of VOP is 78 mAh/g. CTA^+ cations are intercalated in VOP to enlarge the interlayer spacing during the first discharging cycle. The good electrochemical characteristics are attributed to the large interlayer spacing from intercalation of PEDOT and CTA^+ cations, consequently facilitating migration of the intercalated species (Mg^{2+} and $MgCl^+$) (Fig. 3d and e). Meanwhile, the conductive PEDOT pillar not only improves the electrical conductivity, but also stabilizes the layered structure. In future research, adjusting the type and amount of intercalated species for interlayer regulation may further improve the magnesium storage capability.

In addition to the thermodynamically stable phase (α-V_2O_5), V_2O_5 exists in several metastable polymorphs such as β-, γ′-, δ-, ε-, and ζ-V_2O_5 and some of them have potential in RMBs. Based on first-principles calculation, Sai Gautam et al. have found that the Mg diffusion barrier of δ-V_2O_5 (~0.6−0.8 eV) is lower than that of α-V_2O_5 (~0.975−1.1 eV) [63]. Kulish et al. have revealed that β-V_2O_5 has a smaller Mg diffusion barrier (0.65 eV) than α-V_2O_5 [64]. Trocoli et al. have recently reported that β-V_2O_5 has a large discharge capacity of over 400 mAh/g in the 0.1 M $Mg(ClO_4)_2$/AN electrolyte but large voltage hysteresis [65]. Banerjee et al. have shown that ε-V_2O_5 and ζ-V_2O_5 in RMBs have higher average voltages of 3.28 V and 2.92 V besides smaller Mg diffusion barriers of 0.62−0.86 eV and 0.21−0.24 eV, respectively, in comparison with α-V_2O_5 (2.59 V, 1.15−1.23 eV) [66]. ζ-V_2O_5 nanowires are synthesized by leaching Ag ions from β-$Ag_{0.33}V_2O_5$ and the ability of ζ-V_2O_5 to accommodate Mg ions has been demonstrated (Fig. 3f) [60,67]. In the 0.2 M Mg $(TFSI)_2$/PC electrolyte, ζ-V_2O_5 nanowires show a capacity of 90 mAh/g after 100 cycles at 6 mA/g and 50 °C [60]. However, large voltage hysteresis is observed even at small current densities. In order to improve magnesium storage, Johnson et al. have raised the temperature and reduced the size of ζ-V_2O_5 and the nanoscale ζ-V_2O_5 (~100 nm) shows an enhanced capacity of 130 mAh/g in conjunction with reduced voltage hysteresis at 15 mA/g and 110 °C in the 0.5 M Mg $(TFSI)_2$/$PY_{14}TFSI$ electrolyte [68]. The research of metastable V_2O_5 polymorphs as cathode materials is still in its initial stage and the magnesium storage mechanism and optimization need more research in the future.

Amorphous V_2O_5 has been investigated as cathode materials for RMBs. For example, Cheng et al. have fabricated amorphous V_2O_5 nanoclusters with a size below 10 nm on porous carbon and the materials show attractive magnesium storage capacity in 0.2 M $[Mg_2(\mu\text{-}Cl)_2(DME)_4][AlCl_4]_2$/DME electrolyte with Mg being the anode [69]. At low current density, the amorphous V_2O_5 nanoclusters/porous carbon composite has a high initial capacity of 180 mAh/g, which is equivalent to ~350 mAh/g based on the mass of V_2O_5. Even at 640 mA/g, the composite shows a capacity of more

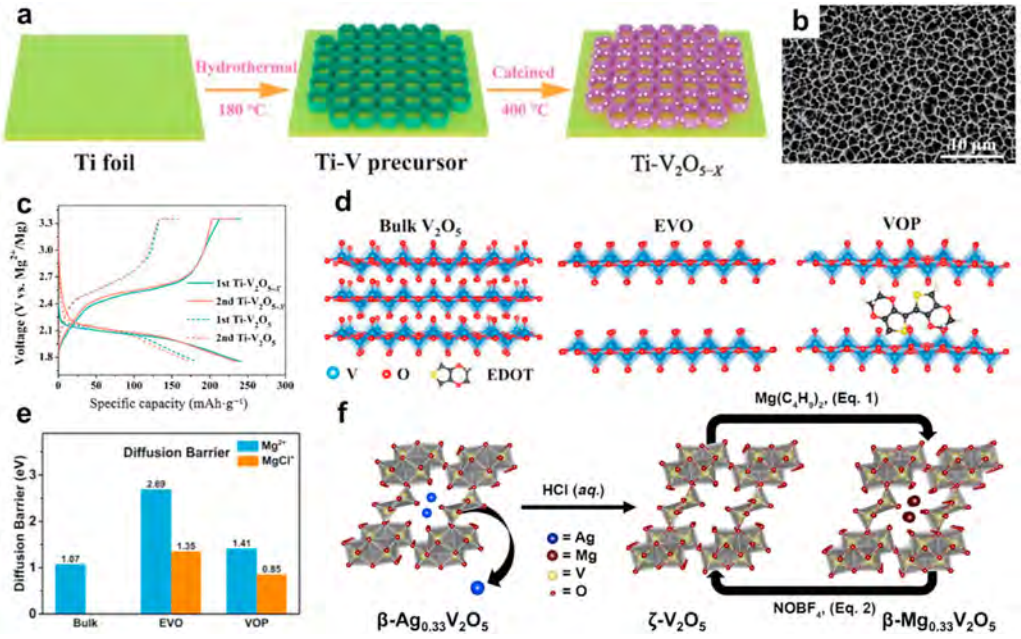

Fig. 3. V_2O_5-based cathode materials for RMBs. (a) The synthesis schematic and (b) Scanning electron microscopy (SEM) image of Ti−V_2O_{5-x}. (c) Charging/discharging curves s of Ti−V_2O_{5-x} and Ti−V_2O_5 in 0.5 M $Mg(ClO_4)_2$/AN with AC as the anode at 100 mA g^{-1} [58]. (d) Schematic of the structure of pristine α-V_2O_5 (bulk V_2O_5), expanded α-V_2O_5 (EVO) and VOP. (e) Diffusion barriers of Mg^{2+} and $MgCl^+$ in these structures [59]. (f) Schematic illustration of the synthesis of ζ-V_2O_5 and reversible chemical Mg-ion intercalation process [60].

than 100 mAh/g. Unfortunately, the cycling stability is still unsatisfactory because of detachment of the nanoclusters from porous carbon. Kim et al. have shown that amorphous V_2O_5 has higher magnesium storage capacity (~180 mAh/g) than crystalline α-V_2O_5 (under 50 mAh/g) [70]. However, Henry et al. has demonstrated improved capacity for a larger water content [71]. After dehydration in 120 °C for 12 h, the capacity of amorphous V_2O_5 thin film decreases to less than 25 mAh/g even at a small current density of 18 mA/g. Whether the amorphous structure is beneficial to magnesium storage for V_2O_5 needs to be confirmed.

2.2. $V_2O_5{\cdot}nH_2O$

$V_2O_5{\cdot}nH_2O$ (hydrated V_2O_5) has a layered structure consisting of two [VO_6] octahedron layers and it is often referred to as bilayered V_2O_5 (Fig. 1b). The presence of interlayered water (or residual organic species) increases the interlayer spacing of $V_2O_5{\cdot}nH_2O$ giving rise to fast and reversible intercalation/deintercalation of Mg-ions. Novák et al. have reported electrochemical intercalation of Mg ions in the V_2O_5 xerogel ($V_2O_5{\cdot}nH_2O$) [39]. The materials show a high initial capacity of about 170 mAh/g in both the $MgCl_2$/$AlCl_3$/EMIC melt and 1 M $Mg(ClO_4)_2$/AN, but the capacity decays rapidly during cycling. Le et al. have studied chemical intercalation of Mg ions in the V_2O_5 aerogel ($V_2O_5{\cdot}nH_2O$) with an interlayer spacing of 1.25 nm using dibutylmagnesium [72]. Two moles of Mg^{2+} can be chemically intercalated into 1 mol of V_2O_5 aerogel ($V_2O_5{\cdot}nH_2O$) and the estimated energy density is as high as 1200 Wh/kg. Imamura et al. have synthesized a V_2O_5 xerogel/C composite with a large interlayer spacing of 1.42 nm and demonstrated that 1.84 mol of Mg can be intercalated into 1 mol of the V_2O_5 xerogel in the 1 M $Mg(ClO_4)_2$/AN electrolyte corresponding to a specific capacity of 540 mAh $(g\text{-}V_2O_5)^{-1}$ [73,74]. The capacity of the V_2O_5 xerogel/C composite is 270 mAh $(g\text{-}V_2O_5)^{-1}$ after 35 cycles at 17 A $(g\text{-}V_2O_5)^{-1}$. Nonetheless, the mass loading of the V_2O_5 xerogel is too low (~0.25 mg/cm^2) and some researchers have question the current densities presented in this paper [75,76]. We also believe that the unit of current density in the original paper is wrong, it should be it should be mA/g instead of A g^{-1}. The V_2O_5 xerogel and S-doped V_2O_5 xerogel prepared by Inamoto et al. also have a high capacity of over 400 mAh/g albeit poor cycling stability [77,78]. These early works demonstrate that $V_2O_5{\cdot}nH_2O$ is a high-capacity cathode materials for RMBs, although the cycling stability needs to be improved.

The water content in $V_2O_5{\cdot}nH_2O$ plays an important role in the magnesium storage capacity and An et al. have investigated the effects of water [24]. When n in $V_2O_5{\cdot}nH_2O$ decreases from 1.35 to 0.43, the capacity at 100 mA/g diminishes from 210 mAh/g to 60 mAh/g, but the interlayer spacing only decreases from 11 Å to 10 Å (Fig. 4a). This is due to the shielding effect of interlayer water. The $V_2O_5{\cdot}1.42H_2O$ nanowire/graphene composite shows a capacity of ~320 mAh/g at 50 mA/g (Fig. 4b), rate performance of ~100 mAh/g at 2 A/g, and 80% capacity retention after 200 cycles in 0.3 M Mg $(TFSI)_2$/AN. The outstanding magnesium storage characteristics of the $V_2O_5{\cdot}1.42H_2O$ nanowire/graphene composite stems from the shielding effect of water (Fig. 4c), good electrical conduction of graphene, and short diffusion distance in the nanowires (Fig. 4d). Ceder et al. have observed that each Mg atom is bonded to four O_w atoms of crystal water and two O_x atoms of the VO_x polyhedron in magnesiated $V_2O_5{\cdot}nH_2O$ ($Mg_{0.5}V_2O_5{\cdot}nH_2O$) based on first-principles calculation [80]. The Mg intercalation potential of $V_2O_5{\cdot}nH_2O$ in a wet electrolyte is calculated to be about 0.15 V higher than that in an anhydrous electrolyte.

Although $V_2O_5{\cdot}nH_2O$ has a high magnesium storage capacity, the poor cycling stability hampers practical application. Pre-intercalation can improve the stability of $V_2O_5{\cdot}nH_2O$ by taking advantage of the pillar effect of pre-intercalated cations. Considering that cation pre-intercalated $V_2O_5{\cdot}nH_2O$ belongs to the vanadate family, the related investigations are summarized in the section of vanadates in this paper.

Organic-intercalated $V_2O_5{\cdot}nH_2O$ has been investigated as cathode materials for RMBs. Perera et al. have fabricated the poly (ethylene oxide) (PEO) intercalated $V_2O_5{\cdot}nH_2O$ composite in which the intercalated PEO expands the interlayer spacing and shields the interactions between Mg ions and host to facilitate migration of Mg ions [81]. The PEO-intercalated $V_2O_5{\cdot}nH_2O$ composite exhibits a 5-fold enhancement in the magnesium storage capacity and 2-fold enhancement in the Mg diffusion coefficient compared to $V_2O_5{\cdot}nH_2O$. However, excessive PEO in the interlayer may hinder Mg diffusion and occupy Mg storage sites. Intercalation of PEO may lower the electrical conductivity due to the insulating nature of PEO. Zuo et al. have prepared conductive organic polymer polyaniline (PANI) intercalated $V_2O_5{\cdot}nH_2O$ (Fig. 4e) [79]. The intercalated PANI not only increases the interlayer spacing, but also improves the electrical conductivity. Consequently, the PANI-intercalated $V_2O_5{\cdot}nH_2O$ displays reversible capacities of over 270 mAh/g at 100 mA/g in 0.3 M Mg $(TFSI)_2$/AN (Fig. 4f) and 80 mAh/g after 500 cycles at a high current density of 4 A/g. In the 0.2 M $Mg(CF_3SO_3)_2$—$MgCl_2$—$AlCl_3$/DME electrolyte with Mg being the anode, PANI-intercalated $V_2O_5{\cdot}nH_2O$ shows a capacity of 115 mAh/g at 100 mA/g, but the average discharge voltage is lower than 1.0 V. Yang et al. have studied the electrochemical properties of PANI-intercalated $V_2O_5{\cdot}nH_2O$ in the APC/THF electrolyte containing 1 M LiCl with Mg being the anode [82]. A high reversible capacity of 361 mAh/g is obtained at 20 mA/g and it remains at 249 mAh/g after 200 cycles. Yang et al. claimed that the main capacity is contributed by Mg intercalation/de-intercalation and Li ions may also promote migration of Mg ions. However, this is contradictory to the reaction mechanism of vanadium-based oxides in the Mg^{2+}/Li^+ hybrid electrolyte described by others [83–87] and more in-depth investigations are needed to elucidate the mechanism.

$V_2O_5{\cdot}nH_2O$ shows a high capacity in the Mg $(ClO_4)_2$-based and Mg $(TFSI)_2$-based electrolytes but these electrolytes are incompatible with Mg anodes. One solution is to replace Mg with other materials. For instance, Tepavcevic et al. have prepared a battery composed of the magnesiated $V_2O_5{\cdot}nH_2O$ cathode, $Mg(ClO_4)_2$/AN electrolyte, and Sn anode [88]. The battery has a capacity of over 100 mAh/g (based on the mass of $V_2O_5{\cdot}nH_2O$) after 50 cycles but the design does not capitalize on the advantages of Mg anodes such as the high capacity, low cost, and abundant resource. Other possibilities include better electrolytes and artificial interfaces on Mg anodes in Mg/$V_2O_5{\cdot}nH_2O$ batteries but more work is needed.

2.3. Other vanadium oxides

Similar to V_2O_5, VO_2 has several polymorphs such as VO_2(R), VO_2(M), VO_2(T), VO_2(A), VO_2(B), and VO_2(C). However, VO_2 has attracted little attention in the RMBs field. Kulish et al. have carried out first-principles investigations on VO_2(R) and VO_2(B) as cathode materials in RMBs and found that the Mg diffusion barrier in VO_2(R) is only 0.33 eV, which is much lower than that in α-V_2O_5 (>1 eV) [64]. This work reveals the potential of VO_2(R) as cathode materials in RMBs, although more evidence has not been reported. Luo et al. have studied the electrochemical properties of VO_2(B) nanorods and nanosheets in 1 M $Mg(ClO_4)_2$/AN [89]. The VO_2(B) nanorods show higher capacity and better cycling stability than the nanosheets. At 25 mA/g, the initial discharge capacity of the VO_2(B) nanorods is 391 mAh/g, which corresponds to intercalation of 0.61 Mg per VO_2(B). However, the capacity of VO_2(B) is very low in the 0.25 M APC/THF electrolyte [84].

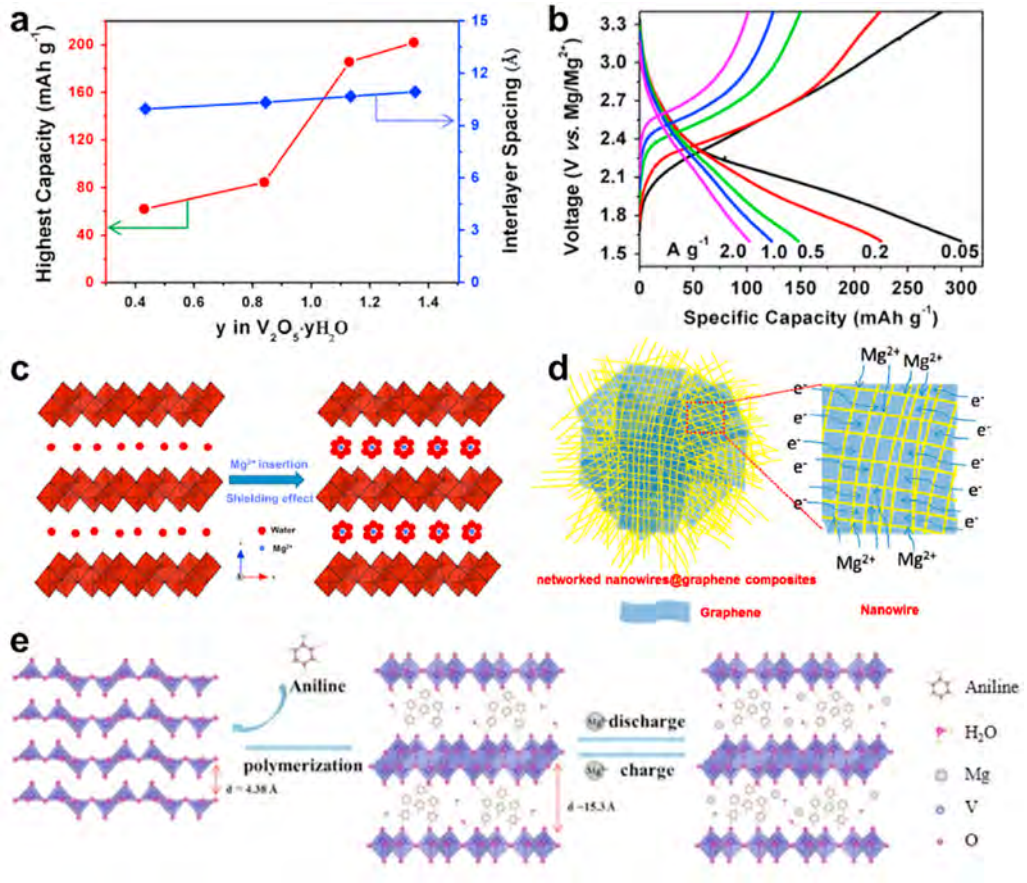

Fig. 4. $V_2O_5 \cdot nH_2O$-based cathode materials for RMBs. (a) Capacities and interlayer spacings of $V_2O_5 \cdot nH_2O$ containing different amounts of water, and (b) charging/discharging curves of the $V_2O_5 \cdot 1.42H_2O$ nanowire/graphene composite in 0.3 M Mg $(TFSI)_2$/AN with AC as the anode. Schematic illustration of the structural advantages of $V_2O_5 \cdot nH_2O$ and $V_2O_5 \cdot nH_2O$ nanowire/graphene composites [24]. (e) Schematic illustration of the synthesis and Mg storage process of PANI-intercalated $V_2O_5 \cdot nH_2O$ [79].

$H_2V_3O_8$ ($V_3O_7 \cdot H_2O$) has a layered structure formed by stacking V_3O_8 layers with corner- or edge-shared VO_6 octahedrons and VO_5 square pyramids (Fig. 1d). Hydrogen in the interlayer expands the interlayer spacing to foster intercalation and migration of Mg ions. Tang et al. have investigated magnesium storage in $H_2V_3O_8$ nanowires [83]. In the 0.5 M $Mg(ClO_4)_2$/AN electrolyte, the $H_2V_3O_8$ nanowires exhibit a high initial capacity of ~300 mAh/g at 50 mA/g and the capacity remains at 261.2 mAh/g after 20 cycles. However, Rastgoo-Deylami et al. have reported that the capacity of $H_2V_3O_8$ nanowires at 10 mA/g and 25 °C is only 80 mAh/g in 0.5 M $Mg(ClO_4)_2$/AN with a water concentration of 48 ppm, but the capacity increases to ~260 mAh/g when the water concentration is increased to 5790 ppm [90]. By raising the temperature to 60 °C, the capacities of $H_2V_3O_8$ nanowires go up to 231 mAh/g at 10 mA/g and 132 mAh/g after 100 cycles at 40 mA/g. The discharged product is $Mg_{0.97}H_2V_3O_8$, suggesting the Mg intercalation contributes to the capacity and the unit-cell volume change of $H_2V_3O_8$ after Mg intercalation is only 0.35%.

V_6O_{13} is composed of alternating single and double [VO_6] octahedron layers (Fig. 1e) and has metallic properties such as high electrical conductivity at room temperature. Bruce et al. have observed that only 0.48 mol of Mg can be chemically intercalated into 1 mol of V_6O_{13}, corresponding to a low capacity of ~50 mAh/g [91]. Wang et al. have investigated the electrochemical performance of V_6O_{13} nanosheets in 1 M $Mg(ClO_4)_2$/AN electrolyte and observed a high capacity of 324 mAh/g [92]. The V_6O_{13} nanosheets show a capacity of 200 mAh/g after 30 cycles at 40 mA/g, but the average discharge potential is lower than 1.0 V (*vs.* Mg^{2+}/Mg) yielding a smaller energy density compared to other vanadium oxides.

V_2O_3 has a rhombohedral corundum-type crystal structure with a three-dimensional V–V framework and the V atoms form distorted [VO_6] octahedrons with surrounding O atoms (Fig. 1f). Pei et al. have prepared V_2O_3@reduced graphene oxide (rGO) microspheres [93]. In the 0.3 M Mg $(TFSI)_2$/AN electrolyte, the V_2O_3@rGO microspheres show a high capacity of 291.3 mAh/g at 50 mA/g and at 2000 mA/g, the capacity is still 185.3 mAh/g and superior to that of pure V_2O_3 (~80 mAh/g). The V_2O_3@rGO microspheres exhibit excellent cycling stability manifested by capacity retention of 88.5% after 1000 cycles at 500 mA/g. *In situ* XRD and *ex situ* XPS disclose that the magnesium storage mechanism of V_2O_3 is the single-phase solid solution reaction based on the V^{3+}/V^{2+} redox couple.

Some non-stoichiometric vanadium oxides are suitable cathode materials for RMBs. Jiao et al. have studied octadecylamine intercalated VO_x nanotubes (VO_x-NTs) in 0.25 M $Mg(AlBu_2Cl_2)_2$/THF [94,95]. The VO_x-NTs have a low capacity of 75 mAh/g at a low current density of 5 mA/g. Cu doping is performed to improve the magnesium storage capacity of VO_x-NTs and the $Cu_{0.1}$-doped VO_x-NTs show an improved capacity of 120 mAh/g [96]. Kim et al. have evaluated the electrochemical properties of VO_x-NTs in 0.5 M $Mg(ClO_4)_2$/AN as well as effects of octadecylamine [97]. The VO_x-NTs with a high concentration of octadecylamine (HT-VO_x) have lower charge transfer resistance and better cycling stability than VO_x-NTs with a low concentration of octadecylamine (LT-VO_x) due to the presence of V^{3+} in HT-VO_x but not in LT-VO_x. At 60 mA/g, HT-VO_x shows capacities of 218 mAh/g initially and 150 mAh/g after 20

cycles. Christensen et al. have investigated the structural evolution of dodecylamine-intercalated VO_x nanotubes (C_{12}-VO_x-NTs) during Mg intercalation/deintercalation by *in situ* XRD and *in situ* total X-ray scattering [98]. Linear expansion/contraction of the interlayer spacing during reduction/oxidation of vanadium is observed during Mg intercalation/deintercalation. Intercalation of Mg ions is incompletely reversible and responsible for the capacity decay.

In summary, investigations on vanadium oxides as cathode materials for RMBs have mainly focused on V_2O_5 and $V_2O_5 \cdot nH_2O$. The layered structure is beneficial to diffusion and storage of Mg ions. Theoretically, V_2O_5 and $V_2O_5 \cdot nH_2O$ can achieve high capacities of more than 500 mAh/g based on complete utilization of the V^{5+}/V^{4+} and V^{4+}/V^{3+} redox couples. Experimentally, some vanadium oxides have high capacities of over 300 mAh/g, but suffer from the poor cycling stability and rate performance. In recent years, efforts have been made to improve the electrochemical properties of vanadium oxides. A cycling life of more than 200 or even 500 cycles has been demonstrated but more improvement is necessary for commercial applications. Notably, good cycling and rates have been achieved from vanadium oxides with Mg anodes by the interlayer regulation strategy. This demonstrates the possibility of obtaining high-performance RMBs based on Mg metal anodes and vanadium oxide cathodes, although the working voltage is still smaller than the expected one. We believe that high-performance Mg-vanadium oxide batteries can be produced in the future by the proper cathode optimization, electrolyte design, and anode modification.

3. Vanadates

Vanadates are derivatives of vanadium oxides comprising other cations. Facile distortion of V—O polyhedrons and rich valence states of V endow the V—O structure with the ability to combine with different amounts and types of cations. Hence, there are many members in the vanadate family. Based on the types of combined cations, vanadates can be classified as alkali metal vanadates, alkali earth metal vanadates, transition metal vanadates, and other vanadates. In this section, recent research activities on vanadates as cathode materials for RMBs are described.

3.1. Alkali metal vanadates

Novák et al. first reported the electrochemical Mg intercalation of $NaV_3O_8 \cdot (H_2O)_y$ [99]. $NaV_3O_8 \cdot (H_2O)_y$ has capacities of 80 mAh/g and 210 mAh/g in 0.5 M $Mg(ClO_4)_2$/PC and 1 M $Mg(ClO_4)_2$ + 2 M H_2O/AN, respectively, but the capacity decays rapidly during cycling. $LiV_3O_8 \cdot (H_2O)_y$, $NaV_3O_8 \cdot (H_2O)_y$, and $KV_3O_8 \cdot (H_2O)_y$ exhibit a similar electrochemical Mg ion intercalation behavior in $MgCl_2$/$AlCl_3$/EMIC molten salt [39]. $NaV_3O_8 \cdot (H_2O)_y$ has a capacity of about 110 mAh/g in the first cycle and >80 mAh/g during long-term cycling. However, the detailed cycling performance of $NaV_3O_8 \cdot (H_2O)_y$ has not been reported. Rashad et al. have synthesized $NaV_3O_8 \cdot 1.69H_2O$ nanobelts and investigated the electrochemical properties in 0.4 M APC/THF [100]. At 10 mA/g, the $NaV_3O_8 \cdot 1.69H_2O$ nanobelts show a capacity of 110 mAh/g. The capacity is 40 mAh/g after 100 cycles at 50 mA/g and capacity retention is about 80%. Sun et al. have studied the magnesium storage performance of $Na_2V_6O_{16} \cdot 1.63H_2O$ (Fig. 5a) nanowires [101]. In 0.5 M Mg $(TFSI)_2$/DME electrolyte, the $Na_2V_6O_{16} \cdot 1.63H_2O$ nanowires show a high capacity of 228 mAh/g at 20 mA/g (Fig. 5b) and excellent cycling stability with a capacity retention of 71% after 450 cycles at 200 mA/g. In contrary, $Na_2V_6O_{16}$ without interlayered water has a capacity of less than 50 mAh/g and first-principles calculation demonstrates that interlayer water facilitates Mg intercalation. However, the rate performance is still unsatisfactory and the capacity decreases to less than 50 mAh/g when the current density is increased to 300 mA/g.

Recently, Wang et al. have observed that $NaV_8O_{20} \cdot nH_2O$ (Fig. 5c) nanobelts show excellent electrochemical properties in the ether—water electrolyte consisting of 1 M $Mg(ClO_4)_2$ in tetraethylene glycol dimethyl ether (TEGDME) and water with a volume ratio of 4:1 [102]. In the ether—water electrolyte, $NaV_8O_{20} \cdot nH_2O$ nanobelts have a high capacity of 350 mAh/g at 300 mA/g (Fig. 5d), which is higher than that in 1 M $Mg(ClO_4)_2/H_2O$ and 1 M $Mg(ClO_4)_2$/TEGDME (below 200 mAh/g). At a current density of 3 A/g, the capacity is 94.3 mAh/g. Moreover, the capacity remains 81.7 mAh/g after 1000 cycles at 1.5 A/g. In comparison, the $NaV_8O_{20} \cdot nH_2O$ nanobelts exhibit fast capacity decay in $Mg(ClO_4)_2/H_2O$ and low capacity in $Mg(ClO_4)_2$/TEGDME. The excellent electrochemical performance can be attributed to the synergistic effects of TEGDME and water. TEGDME suppresses dissolution of $NaV_8O_{20} \cdot nH_2O$ (Fig. 5e) and ensures a wide electrochemical window by coordinating with free water to suppress the reactivity. At the same time, the shielding effect rendered by water enhances diffusion of Mg ions. Although excellent magnesium storage properties have been achieved using the ether-water electrolyte, this electrolyte system may be incompatible with Mg anodes due to the high water content. Nevertheless, this work shows that electrolyte regulation is an effective strategy to improve Mg storage in vanadates. Future research should consider the compatibility between electrolytes and both vanadium-based cathode materials and Mg anodes at the same time.

Besides hydrated sodium vanadates, some anhydrous alkali metal vanadates are suitable cathode materials for RMBs. Tang et al. have investigated the magnesium storage capacity of AV_3O_8 (A = Li, Na, or K) in 0.5 M $Mg(ClO_4)_2$/AN [103]. At 100 mA/g, LiV_3O_8 shows the highest capacity (252 mAh/g) despite fast capacity fading (capacity retention of 42.2% after 30 cycles). NaV_3O_8 has a slightly smaller capacity (204 mAh/g) but better cycling stability (capacity retention of 85.78% after 30 cycles) (Fig. 5f and g). Different from LiV_3O_8 and NaV_3O_8, KV_3O_8 exhibits a low capacity (below 40 mAh/g) due to the different layered structure. First-principles calculation indicates that migration of Na in NaV_3O_8 is more difficult than that of Li in LiV_3O_8 (Fig. 5h), implying better structural stability of NaV_3O_8 compared to LiV_3O_8, which is responsible for the enhanced cycling stability of NaV_3O_8. After 100 cycles at 500 mA/g, NaV_3O_8 shows capacity retention of 88.3%. Cabello et al. have studied NaV_6O_{15} as cathode materials in RMBs [104]. In the 1 M $Mg(ClO_4)_2$/AN electrolyte with Mg as the anode, NaV_6O_{15} shows an initial capacity of 90 mAh/g, but it decreases to almost 0 mAh/g after 25 cycles. In the three-electrode system with Mg as both counter and reference electrodes, the maximum capacity increases to more than 200 mAh/g, but the cycling stability is still poor on account of passivation of the Mg electrode in $Mg(ClO_4)_2$/AN. Wu et al. have studied NaV_6O_{15} in 0.5 M $Mg(ClO_4)_2$/AN with AC as the anode and good cycling stability is observed [105]. After 100 cycles at 20 mA/g, the capacity of NaV_6O_{15} is 120 mAh/g but the rate of NaV_6O_{15} is poor. At 200 mA/g and 500 mA/g, NaV_6O_{15} shows low capacities of 52.3 and 27.2 mAh/g, respectively. Reversible Mg intercalation/deintercalation in NaV_6O_{15} with minor layer spacing change is revealed and density-functional theory (DFT) calculation demonstrates that the intercalated Mg ions tend to occupy the semi-occupied Na sites in NaV_6O_{15}. Compared to hydrated sodium vanadates, anhydrous sodium vanadates usually have inferior electrochemical properties attributable to the smaller interlayer spacing.

Based on DFT calculations, Hannah et al. have found that the $CaFe_2O_4$-type NaV_2O_4 and $NaV_{1.25}Ti_{0.75}O_4$ have Mg diffusion barriers below 0.4 eV after desodiation [106]. However, $CaFe_2O_4$-type NaV_2O_4 is only stable at high pressure. On the contrary, Ti-substituted NaV_2O_4 ($NaV_{1.25}Ti_{0.75}O_4$) is stable in the $CaFe_2O_4$-type

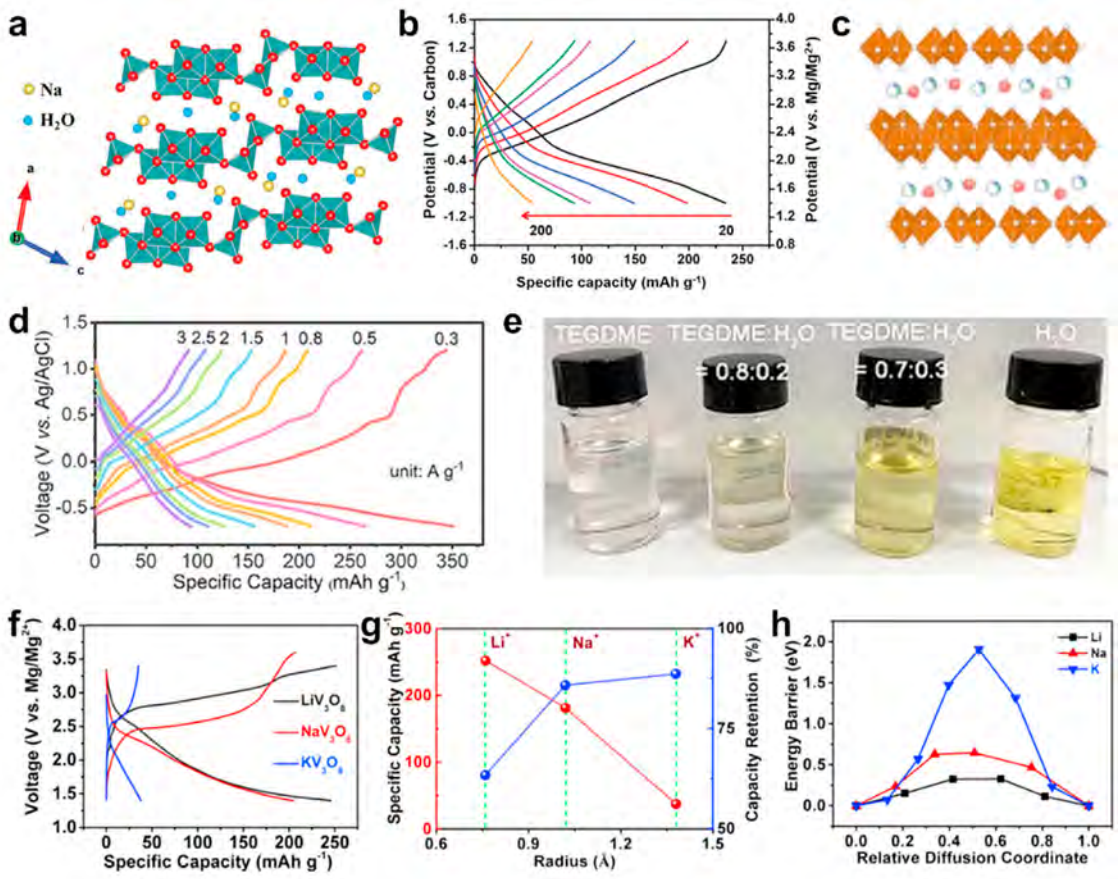

Fig. 5. Alkali metal vanadates for RMBs. (a) Crystal structure of $Na_2V_6O_{16}\cdot 1.63H_2O$ and (b) charge discharge curves of $Na_2V_6O_{16}\cdot 1.63H_2O$ nanowires in 0.5 M Mg $(TFSI)_2$/DME electrolyte with AC as anode [101]. (c) Crystal structure of $NaV_8O_{20}\cdot nH_2O$. (d) Charging/discharging curves of $NaV_8O_{20}\cdot nH_2O$ nanobelts at different current densities in the $Mg(ClO_4)_2$/ether–water hybrid electrolyte (TEGDME: H_2O = 0.8: 0.2). Tests conducted on the three-electrode system with Pt as the counter electrode and Ag/AgCl as the reference electrode. (e) Photographs of four different electrolytes after the rate test of $NaV_8O_{20}\cdot nH_2O$ nanobelts: TEGDME, TEGDME/H_2O = 0.8:0.2, TEGDME/H_2O = 0.7:0.3, H_2O-based electrolyte [102]. (f) Charging/discharging curves of AV_3O_8 (A = Li, Na, or K) at 100 mA/g in the 0.5 M $Mg(ClO_4)_2$/AN electrolyte with AC as both the counter and reference electrodes. (g) (h) Diffusion energy barriers of Li, Na, and K in the corresponding AV_3O_8 [103].

structure at ambient pressure. Sun et al. have synthesized $CaFe_2O_4$-type $NaV_{1.25}Ti_{0.75}O_4$ and determined the magnesium storage capacity of the desodiated product [107]. $Na_{0.25}V_{1.25}Ti_{0.75}O_4$ obtained from $NaV_{1.25}Ti_{0.75}O_4$ by chemical desodiation in the I_2/AN solution has an initial capacity of 80 mAh/g in 0.5 M $Mg(CB_{11}H_{12})_2$/tetraglyme with Mg metal being the anode at 5 mA/g and 60 °C, but the capacity is only 40 mAh/g in subsequent cycles due to the electrochemically inactive amorphous phase on the surface.

3.2. Alkali earth metal vanadates

Investigation of alkali earth metal vanadates as cathode materials for RMBs has primarily focused on magnesium vanadates. Novák et al. have studied the magnesium storage properties of $Mg(V_3O_8)_2\cdot(H_2O)_y$ in $MgCl_2/AlCl_3$/EMIC molten salt, which are better than those of $NaV_3O_8\cdot(H_2O)_y$ [39,99]. $Mg(V_3O_8)_2\cdot(H_2O)_y$ has capacities of 150 mAh/g initially and 60 mAh/g after 50 cycles. In addition, some $Mg_xV_2O_5\cdot nH_2O$ materials have been synthesized and used as cathode materials for RMBs [108–110]. For example, Xu et al. have prepared $Mg_{0.3}V_2O_5\cdot 1.1H_2O$ nanowires with an interlayer spacing of 1.19 nm (Fig. 6a) [110]. In the 0.3 M Mg $(TFSI)_2$/AN electrolyte, the $Mg_{0.3}V_2O_5\cdot 1.1H_2O$ nanowires show a reversible capacity of 164 mAh/g at 0.1 A/g (Fig. 6b) and no obvious decay in 500 cycles, whereas the capacity of $V_2O_5\cdot nH_2O$ drops quickly to 30 mAh/g in 200 cycles. Moreover, the $Mg_{0.3}V_2O_5\cdot 1.1H_2O$ nanowires exhibit long cycling life of 10,000 cycles with capacity retention of over 80%. The enhanced properties are related to the shielding effect of interlayer water and better electrical conductivity (Fig. 6c). Highly reversible Mg intercalation/deintercalation in $Mg_{0.3}V_2O_5\cdot 1.1H_2O$ occurs with small structural variation as revealed by *in situ* XRD, *ex situ* XANES, and NMR. This work demonstrates the possibility of obtaining high-rate and long-life vanadium-based cathode materials for RMBs. Unfortunately, the high capacity of vanadium-based materials has not been exploited in the work.

Recently, spinel MgV_2O_4 has received attention because it contains extractable Mg-ions. DFT calculation predicts that spinel MgV_2O_4 has a working voltage of ~2.5 V, high volumetric capacity of over 1100 Ah/L, as well as small volume change of 7% during charging/discharging [114]. Kuganathan et al. have shown that the Mg diffusion barrier in MgV_2O_4 is 0.52 eV (Fig. 6d) [111]. Hu and coworkers have synthesized MgV_2O_4 nanocrystals and investigated the electrochemical properties in the 0.5 M Mg $(TFSI)_2/PY_{14}TFSI$ electrolyte [112]. At 110 °C, the MgV_2O_4 nanocrystals show a charging capacity of 280 mAh/g when charged to 3.6 V (vs. Mg^{2+}/Mg), corresponding to extraction of 1 mol of Mg for each mole of MgV_2O_4 (Fig. 6f). A discharging capacity of 235 mAh/g is also achieved and the average voltage is about 2.5 V as predicted by Liu et al. [114], but large voltage hysteresis is observed. When the temperature is lowered to 25 °C, the capacity of the MgV_2O_4 nanocrystals

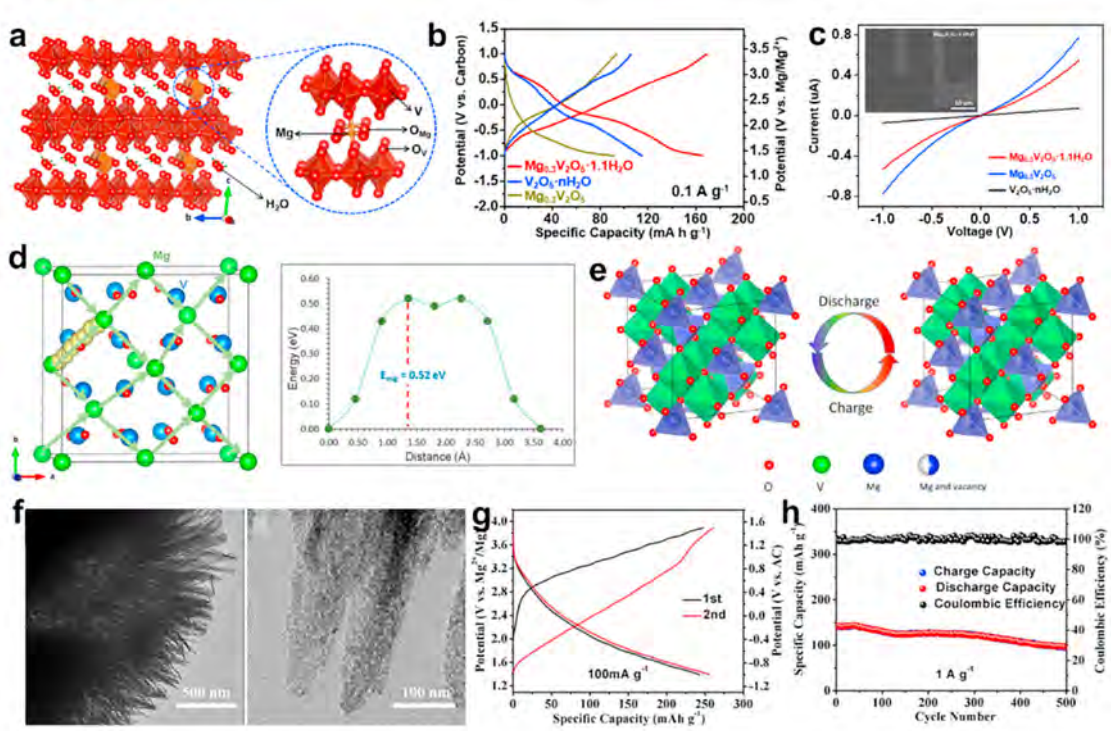

Fig. 6. Alkali earth metal vanadates for RMBs. (a) Crystal structure of $Mg_{0.3}V_2O_5{\cdot}1.1H_2O$. (b) Charging/discharging curves of $Mg_{0.3}V_2O_5{\cdot}1.1H_2O$, $V_2O_5{\cdot}nH_2O$ and $Mg_{0.3}V_2O_5$ at 100 mA/g in the 0.3 M Mg $(TFSI)_2$/AN electrolyte with AC as the anode. (c) I–V curves of $Mg_{0.3}V_2O_5{\cdot}1.1H_2O$, $V_2O_5{\cdot}nH_2O$ and $Mg_{0.3}V_2O_5$ tested by single nanowire devices (insert) [110]. (d) Diffusion pathways and diffusion energy barrier of Mg-ion in spinel MgV_2O_4 [111]. (e) Schematic illustration of structural evolution of spinel MgV_2O_4 during Mg-ion extraction/insertion process [112]. (f) Transmission electron microscopy (TEM) images of $Mg(Mg_{0.5}V_{1.5})O_4$ hierarchical microspheres, (g) charging/discharging curves at 100 mA/g and (h) cycling characteristics at 1 A/g of $Mg(Mg_{0.5}V_{1.5})O_4$ hierarchical microspheres in the 0.3 M Mg $(TFSI)_2$/AN electrolyte with AC as the anode [113].

decreases to 45 mAh/g, but the Coulombic efficiency increases to close to 100% and no obvious capacity decay is observed for 85 cycles. The reversible magnesium extraction/insertion process of MgV_2O_4 accompanied by V^{3+}/V^{4+} redox reaction is revealed (Fig. 6e). Idemoto et al. have investigated the electrochemical properties of $Mg(Mg_{0.5}V_{1.5-x}Ni_x)O_4$ (x = 0, 0.1, 0.2, 0.3) [115]. In the 1 M Mg $(TFSI)_2$/triglyme electrolyte at 90 °C, $Mg(Mg_{0.5}V_{1.4}Ni_{0.1})O_4$ exhibits the highest capacity of 66 mAh/g. To improve the electrochemical properties, Zuo et al. have fabricated $Mg(Mg_{0.5}V_{1.5})O_4$ hierarchical microspheres with nano-contacts consisting of small particles with a size of 10 nm (Fig. 6f) [113]. In the 0.3 M Mg $(TFSI)_2$/AN electrolyte, the $Mg(Mg_{0.5}V_{1.5})O_4$ hierarchical microspheres show a reversible capacity of 250 mAh/g (Fig. 6g). Even at 4 A/g, the capacity is 142 mAh/g and a capacity of 100 mAh/g is maintained after 500 cycles at 1 A/g (Fig. 6h). The $Na_2Ti_3O_7/Mg(Mg_{0.5}V_{1.5})O_4$ full battery with the 0.3 M Mg $(TFSI)_2$/AN electrolyte shows a capacity of 102 mAh/g after 100 cycles at 50 mA/g. Cathode materials containing extractable Mg ions provide the possibility to construct the Mg-ion batteries based on Mg-free anode materials similar to LIBs. However, such Mg-ion batteries may not be competitive compared to LIBs and Na-ion batteries due to the loss of the advantages of Mg anodes.

3.3. Transition metal vanadates

There are different types of transition metal vanadates but only a few are potential cathode materials for RMBs. Kaveevivitchai et al. have prepared the molybdenum vanadate ($Mo_{2.48}VO_{9.93}$) with a microporous structure containing large open channels constructed by three-, six-, and seven-membered rings of [MoO_6] or [VO_6] octahedrons (Fig. 7a), which facilitate intercalation and diffusion of Mg ions [116]. $Mo_{2.48}VO_{9.93}$ has an initial capacity of 379 mAh/g at a current density of 2 mA/g in 0.5 M Mg $(TFSI)_2$/AN electrolyte, corresponding to intercalation of 3.49 mol of Mg for each mole of $Mo_{2.48}VO_{9.93}$ (Fig. 7b). However, the capacity of $Mo_{2.48}VO_{9.93}$ decays swiftly in the initial cycles and drops to 235 mAh/g after 15 cycles. The capacity decay is caused by trapping of Mg ions in the three-membered ring tunnels. The unit cell volume expansion of $Mo_{2.48}VO_{9.93}$ is only 5% after intercalation of 3 Mg per unit. Miao et al. reported that in the 0.4 M APC/THF electrolyte with Mg as the anode, MoV_2O_8 shows a capacity of over 200 mAh/g in the first cycles, but the capacity deteriorates rapidly to less than 50 mAh/g after several cycles [117]. Both molybdenum and vanadium have rich valence states and so molybdenum vanadates can achieve high Mg storage capacity through multi-electron reactions. However, the cycling stability of molybdenum vanadates needs to be improved and the magnesium storage mechanism needs to be studied systematically as well.

Tang et al. have observed transfer of crystalline $FeVO_4$ to the ordered/disordered composite structure during magnesium storage (Fig. 7c) and the ordered/disordered structure enhances the cycling stability [118]. As a result, $FeVO_4$ has excellent cycling stability with capacity retention of ~85% after 1000 cycles at 1 A/g in 0.3 M Mg $(TFSI)_2$/AN electrolyte. $Fe_5V_{15}O_{39}(OH)_9{\cdot}9H_2O$ is also suitable for RMBs. Tang et al. fabricated $Fe_5V_{15}O_{39}(OH)_9{\cdot}9H_2O$ nanosheet arrays on carbon cloth (FVO/CC) as flexible cathodes for RMBs [119]. The carbon cloth provides fast charge transport pathways and prevents the aggregation of nanosheets (Fig. 7d). Consequently, FVO/CC shows better capacity (300 mAh/g), rate capability (120 mAh/g at 2000 mA/g), and cycling stability (70 mAh/g after 5000 cycles) compared to FVO nanosheets. Moreover, the single-phase magnesium storage mechanism with both Fe (Fe^{3+}/Fe^{2+}) and V ($V^{5+}/V^{4+}/V^{3+}$) as redox centers is

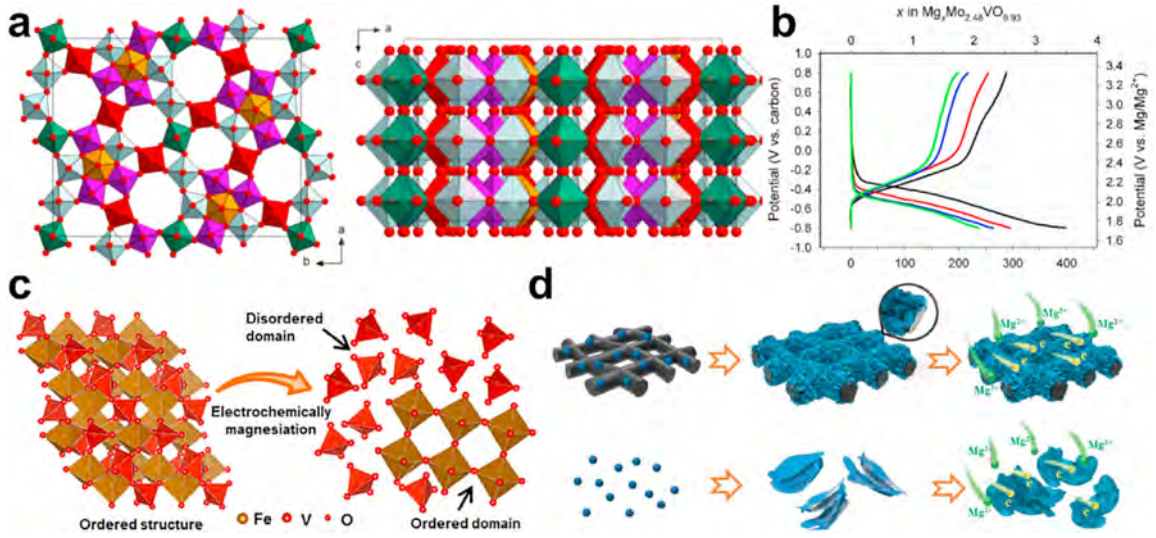

Fig. 7. Transition metal vanadates for RMBs. (a) Crystal structure and (b) Charging/discharging curves of $Mo_{2.48}VO_{9.93}$ in the 0.5 M Mg $(TFSI)_2$/AN electrolyte with AC as both the counter and reference electrodes [116]. (c) Schematic of the structural change of $FeVO_4$ during magnesiation [118]. (d) Schematic showing the synthesis and structural advantages of FeVO/CC [119].

revealed. However, the use of carbon cloth reduces the energy density of the battery system due to the larger inactive component proportion, especially when the loading of active materials is low.

$Mn_{0.04}V_2O_5{\cdot}1.17H_2O$ nanobelts considered as Mn pre-intercalated $V_2O_5{\cdot}1.17H_2O$ nanobelts have been synthesized by Deng et al. [120]. Benefiting from the shielding effect of interlayered water and pillar effect of Mn ions, the $Mn_{0.04}V_2O_5{\cdot}1.17H_2O$ nanobelts show excellent rates (50 mAh/g at 4 A/g) and long cycling life (10,000 cycles) in 0.3 M Mg $(TFSI)_2$/AN electrolyte. Moreover, the single-phase magnesium storage process of $Mn_{0.04}V_2O_5{\cdot}1.17H_2O$ nanobelts with a small volume change is revealed. It is worth noting that there are only a few Mn ions in the $Mn_{0.04}V_2O_5{\cdot}1.17H_2O$, although this brings about better cycling stability than $V_2O_5{\cdot}nH_2O$. Compared to $Mg_{0.3}V_2O_5{\cdot}1.1H_2O$ with a similar crystal structure [110], $Mn_{0.04}V_2O_5{\cdot}1.17H_2O$ has a smaller interlayer spacing (10.9 Å *vs.* 11.9 Å) and lower capacity (145 mAh/g *vs.*164 mAh/g), thereby suggesting that the magnesium storage capacity of vanadate is related to the interlayer spacing, even though the specific relationship needs to be studied in-depth in the future.

3.4. Other vanadates

Besides the aforementioned vanadates, other vanadates including ammonium vanadate and aluminum vanadate have been proposed as cathode materials for RMBs. Esparcia Jr. et al. have investigated the Mg storage behavior of $NH_4V_4O_{10}$ and found that NH_4^+ can be extracted from $NH_4V_4O_{10}$ in the first charging process which expands the interlayer spacing and increases the capacity in subsequent cycles [121]. In 0.5 M $Mg(ClO_4)_2$/AN, $NH_4V_4O_{10}$ shows a reversible capacity of 250 mAh/g in the second cycle at 0.2C (1 C = 210.6 mA/g) after extraction of NH_4^+ in the first charging cycle. However, extraction of NH_4^+ results in fast capacity decay and the capacity decreases to 36.8 mAh/g after 100 cycles at 1 C. After narrowing the electrochemical window to prevent extraction of NH_4^+, enhanced cycling stability with a capacity of 101 mAh/g after 100 cycles at 1 C is accomplished. These results demonstrate that NH_4^+ plays an important role in the structural stability of $NH_4V_4O_{10}$ during Mg intercalation/intercalation. Wei et al. have prepared $(NH_4)_2V_6O_{16}{\cdot}1.5H_2O$ nanobelts as cathode materials for RMBs [122]. In the 0.5 M $Mg(ClO_4)_2$/AN electrolyte, the $(NH_4)_2V_6O_{16}{\cdot}1.5H_2O$ nanobelts show an initial capacity of 100 mAh/g, but the capacity decreases to 63 mAh/g after 50 cycles. Interlayer water plays an important role in magnesium storage in $(NH_4)_2V_6O_{16}{\cdot}1.5H_2O$. The capacity of $(NH_4)_2V_6O_{16}$ without interlayer water is less than 10 mAh/g under the same conditions. Electrochemical analysis and DFT calculation reveal that the interlayer water improves the Mg diffusion kinetics in $(NH_4)_2V_6O_{16}{\cdot}1.5H_2O$.

Tang et al. have prepared urchin-like aluminum vanadate ($H_{11}Al_2V_6O_{23.2}$) microspheres [123]. Similar to the other hydrated layered vanadates, the pillar effect of Al ions in the interlayer of $H_{11}Al_2V_6O_{23.2}$ improves the structural stability and the shielding effect of interlayer water facilitates Mg diffusion. As a result, urchin-like $H_{11}Al_2V_6O_{23.2}$ microspheres show a reversible capacity of 165 mAh/g at 0.1 A/g in 0.3 M Mg $(TFSI)_2$/AN. The urchin-like $H_{11}Al_2V_6O_{23.2}$ microspheres also have excellent capacity retention of 87% after 3000 cycles at 1 A/g.

Compared to vanadium oxides, layered vanadates usually exhibit better cycling stability due to the "pillar effect" of cations in the interlayer. In addition, the vanadium atoms in some vanadates have mixed valences leading to better electronic conductivity and some layered vanadates such as $Mg_{0.3}V_2O_5{\cdot}1.1H_2O$ nanowires have a long lifetime of over 5000 cycles. However, in some vanadates like $NH_4V_4O_{10}$, the interlayered cations are extracted during charging resulting in structural collapse and fast capacity decay. Excellent electrochemical properties have been observed from vanadates in electrolytes that are incompatible with Mg anodes, but the lack of suitable electrolytes compatible with both Mg anodes and vanadates poses a challenge for future development of vanadate cathode materials for RMBs. So far, researches working on vanadate RMB cathodes have mainly screened the materials and there have only been scattered reports on optimizing the electrochemical properties. In the future, different optimization strategies are expected to improve the magnesium storage characteristics of vanadates.

4. Vanadium chalcogenides

4.1. VS_2

VS_2 has a layered structure in which the sandwiched S—V—S layers are stacked by weak van der Waals force. Gregory et al. have

reported that 0.34 mol of Mg ions can be intercalated into 1 mol of VS_2 with an open-circuit potential of 1.71 V (vs. Mg^{2+}/Mg) [38]. Unfortunately, in some electrolytes with high Mg plating/stripping efficiency, pristine VS_2 has small reversible capacities [124–127].

Interlayer regulation is an effective strategy to improve magnesium storage performance of VS_2. For example, Xue et al. have found that 2-ethylhexylamine (2-EHA) intercalated VS_2 nanoflowers with an expanded interlayer spacing of 9.93 Å (Fig. 8a) deliver enhanced electrochemical performance compared to VS_2 nanoflowers without 2-EHA intercalation [125]. In the electrolyte composed of magnesium hexamethyldisilazide and $MgCl_2$ in a mixture of THF and *n*-butyl-*n*-methyl-piperidinium bis((trifluoromethyl)sulfonyl)imide ($Mg(HMDS)_2$-$4MgCl_2$/2THF-$PP_{14}TFSI$) and with Mg metal being the anode, the 2-EHA intercalated VS_2 nanoflowers show a high reversible capacity of 245 mAh/g at 100 mA/g and a capacity of 103 mAh/g is observed at 2000 mA/g (Fig. 8b). The 2-EHA intercalated VS_2 nanoflowers also exhibit good cycling stability such as a capacity of 90 mAh/g after 600 cycles at 1000 mA/g. Intercalation of 2-EHA not only facilitates diffusion of intercalated Mg species by enlarging the diffusion channels and alleviating undesirable electrostatic interactions between the intercalation species and VS_2, but also enhances the structural stability by the pillar effect. Similarly, octylamine and/or NH^{4+} intercalated VS_2 with an expanded interlayer spacing of 10 Å has good electrochemical properties [126]. Besides introducing organic species into the interlayers during synthesis, intercalating organic ions into the interlayers electrochemically can enlarge the interlayer spacing in layered compounds. Zhao et al. have investigated the electrochemical properties of VS_2 nanosheets in the APC/THF electrolyte with the $PP_{14}Cl$ additive and found that PP_{14}^+ ions are intercalated into VS_2 in the first discharging cycle consequently enlarging the interlayer spacing from 0.61 nm to 1.10 nm (Fig. 8c) [128]. The PP_{14}^+ ions remain in the interlayer of VS_2 during subsequent cycling. The VS_2 nanosheets show a high reversible capacity of 348 mAh/g at 20 mA/g in addition to a capacity of 214 mAh/g at 2 A/g. These results demonstrate that VS_2 with expanded interlayer spacing can have good magnesium storage properties. However, the average discharge voltage of VS_2 is lower than 1.0 V which greatly limits the practical prospects.

4.2. VSe_2

The crystal structure of VSe_2 is similar to that of VS_2. However, different from the smaller capacity of pristine VS_2 in the APC/THF electrolyte, microscale VSe_2 shows a reversible capacity of 120 mAh/g in APC/THF or $Mg(AlCl_2EtBu)_2$/THF electrolyte with Mg being the anode (Fig. 8d) [124,129]. Mao et al. have reported that the Mg diffusion barrier of VSe_2 (346 meV) is lower than that of VS_2 (593 meV), which is responsible for the difference in magnesium storage between VSe_2 and VS_2 [124]. The Mg diffusion barriers in MX_2 compounds (M = Ti or V, and X = O, S or Se) with the same layered structure display the decreasing trend of "oxide–sulfide–selenide" (Fig. 8e–g) because of the different electronegativity (O > S > Se) and ionic radii (O^{2-} < S^{2-} < Se^{2-}) of the anions.

Nanometerization is an efficient way to improve magnesium storage in VSe_2. Tao et al. have reported that VSe_2 nanosheet-assembled hierarchical rods have higher magnesium storage

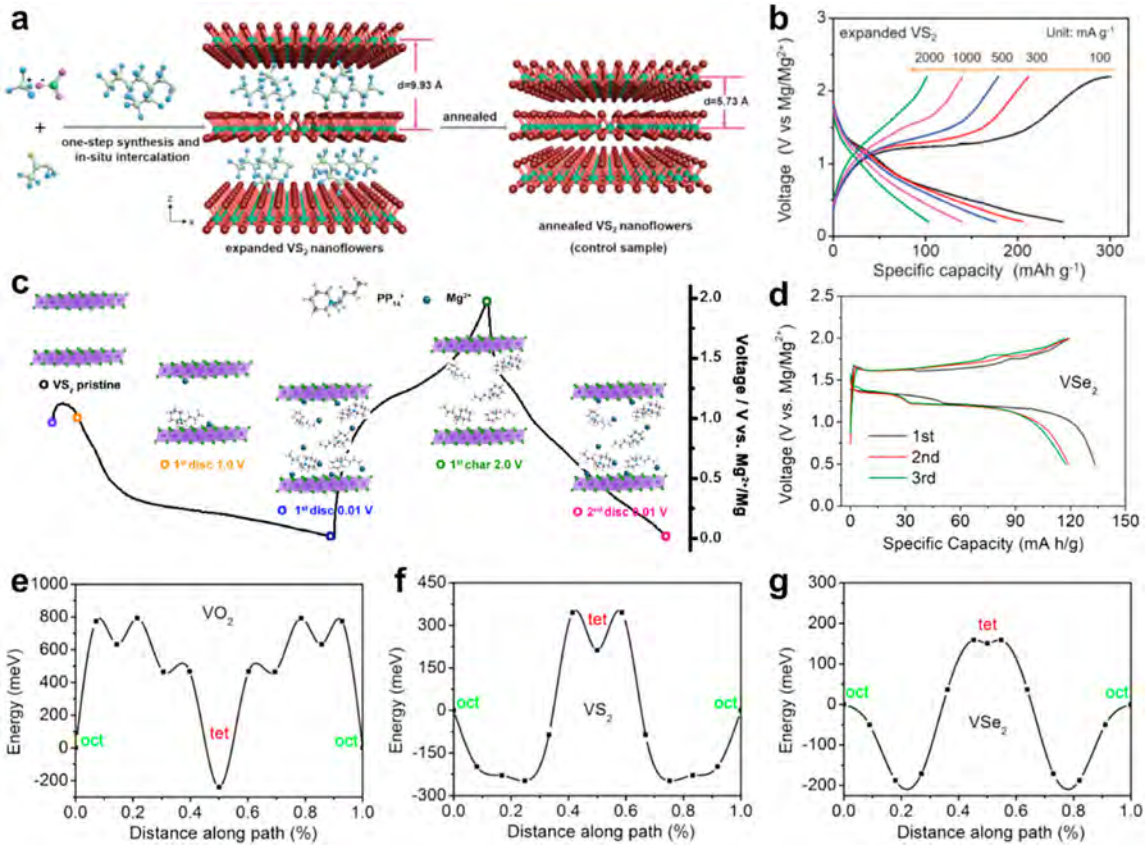

Fig. 8. Vanadium dichalcogenides for RMBs. (a) Schematic illustration of the synthesis and crystal structure of 2-EHA intercalated VS_2 and VS_2. (b) Charging/discharging curves of 2-EHA intercalated VS_2 in the $Mg(HMDS)_2$-$4MgCl_2$/2THF-$PP_{14}TFSI$ electrolyte with Mg metal as the anode [125]. (c) Schematic of the structural change during discharging/charging of VS_2 in the APC/THF electrolyte with the $PP_{14}Cl$ additive [128]. (d) Charging/discharging curves of VSe_2 in the APC/THF electrolyte with Mg metal as the anode. Diffusion energy barriers of Mg-ion in layered (e) VO_2, (f) VS_2, and (g) VSe_2 [124].

capacities than VSe_2 microplates [130]. However, the capacity of VSe_2 nanosheet-assembled hierarchical rods decays rapidly from over 300 mAh/g to about 100 mAh/g in only 30 cycles. Gao et al. have synthesized the VSe_2 nanoparticles/rGO composite as cathode materials for RMBs [131]. In the 0.25 M APC/THF electrolyte with Mg as the anode, the composite shows capacities of 235.5 mAh/g at 50 mA/g, 150 mAh/g after 500 cycles, and 97.8 mAh/g at 1000 mA/g.

4.3. VS_4

VS_4 has the unique chain-like structure with an interchain distance of 5.83 Å (Fig. 9a) and the open channels between chains facilitate Mg diffusion and storage. Wang et al. have investigated the electrochemical properties of VS_4 [132]. The VS_4 nanodendrites exhibit a high initial capacity of ~250 mAh/g at 100 mA/g in the 0.4 M APC/THF electrolyte with Mg metal as the anode. The capacity decreases quickly to 126 mAh/g in five cycles but increases gradually to 177 mAh/g in subsequent cycles. At 500 mA/g, the VS_4 nanodendrites show a capacity of 106 mAh/g. During cycling at 500 mA/g, the capacity of the VS_4 nanodendrites is 75.2 mAh/g after 800 cycles. The unique valence state change in VS_4 is presented in Fig. 9d and e. During discharging, S_2^{2-} in VS_4 is partially reduced to S^{2-}, while V^{4+} is partially oxidized to V^{5+}. Most of the V^{5+} and S^{2-} change back to V^{4+} and S_2^{2-}, respectively, during charging. Li et al. have explained this unique valence state change (Fig. 9b) [133]. The electronic structure of VS_4 can be simplified to the bonding and antibonding orbitals of S^{2-} partially overlapping the V 3 d band. Based on energy level ordering, ten electrons occupy orbitals of S_2^{2-} and one electron occupies the orbital of V^{4+}. During Mg intercalation, two electrons are transferred to the antibonding orbital of S2 σ* causing an unstable state and breaking S—S bonds. Afterwards, the bonding and antibonding orbitals of S_2^{2-} transform to a single broad S3p band that sits completely below the V3d band, leading to electron transfer from V to S and oxidation of V^{4+} to V^{5+}. The reaction of can be described as $1.5Mg^{2+} + 3e^- + VS_4\ [V^{4+}, S_2^{2-}] \leftrightarrow Mg_{1.5}VS_4\ [V^{5+}, S^{2-}]$. Dey et al. have provided new information about the magnesium storage mechanism in VS_4 based on the systematic characterization [134]. As shown in Fig. 9c, at the beginning of discharging (from A to B), a part of VS_4 is converted to $Mg_3V_2S_8\ [V^{5+}, S^{2-}]$ by a cation−anion redox-mediated process. In the next stage (from B to D), the intercalation reaction ($xMg^{2+} + 2xe^- + Mg_{3+x}V_2S_8$) and conversion reaction ($4Mg^{2+} + 8e^- + VS_4 \leftrightarrow V + 4MgS$) take place simultaneously. In the last stage of discharging (from D to E), the conversion reaction becomes dominant.

Recently, efforts have been made to improve the electrochemical properties of VS_4. Various VS_4-based nanocomposites have been proposed to be cathode materials for RMBs. For example, Li et al. have synthesized the VS_4/rGO composite showing a capacity of 440 mAh/g at 50 mA/g in the magnesium tetrakis (hexafluoroisopropanol)borate (Mg [B (hfip)$_4$]$_2$)/DME electrolyte with Mg being the anode [133]. Zhu et al. have fabricated VS_4 nanosheets on carbon-coated Ti_3C_2 MXene (VS_4@Ti_3C_2/C) and investigated the electrochemical characteristics in 0.25 M APC/THF electrolyte with Mg being the anode [135]. VS_4@Ti_3C_2/C shows good cycling stability such as a capacity of 147 mAh/g after 900 cycles at 500 mA/g and capacity retention of 80%. Li et al. have reported the electrochemical properties of the core-shell carbon nanotube (CNT)@VS_4 nanocomposite in the 0.4 M APC/THF electrolyte with the Mg anode [136]. The core-shell CNT@VS_4 nanocomposite shows a capacity of 77.2 mAh/g at 2000 mA/g in addition to capacity retention of 68% after 800 cycles at 500 mA/g.

Besides designing VS_4-based nanocomposites, defect engineering has been employed to enhance the magnesium storage properties of VS_4. Ding et al. have performed Mo doping to expand the interchain distance of VS_4 [137] and generate of sulfur vacancies for better Mg diffusion. VS_4 doped with 3% Mo exhibits a capacity of 140 mAh/g at 20 mA/g in 0.4 M APC/THF with Mg metal being the anode and it is better than that of VS_4 without Mo doping (78 mAh/g). They have also synthesized Mo/O co-doped VS_4 and Mo-doped VS_4/N-doped tubular graphene (N-TG) [138,139]. Mo/O co-doped VS_4 has a capacity of 75.2 mAh/g at 1000 mA/g together with high capacity retention of 92% after 1000 cycles. These modified VS_4-based materials exhibit improved rate performance and cycling stability but smaller reversible capacity, thus rendering them less attractive.

Interchain regulation has been demonstrated to be an efficient strategy to improve the electrochemical properties of VS_4 as cathode materials for RMBs. Pei et al. have conducted electrochemical intercalation of PY_{14}^+ in the APC/THF electrolyte with the $PY_{14}Cl$ additive to expand the interchain distance of VS_4 [140]. The VS_4@rGO composite after PY_{14}^+ intercalation shows a reversible capacity of 268.3 mAh/g at 50 mA/g. At 2000 mA/g, the VS_4@rGO composite after PY_{14}^+ intercalation shows a capacity of 85.9 mAh/g. Intercalation/deintercalation of $MgCl^+$ is the dominant mechanism in PY_{14}^+ intercalated VS_4@rGO in the APC electrolyte during charging/discharging. Ding et al. have reported the K-ion pre-intercalated VS_4 ($K_{0.2}VS_4$)/N-TG cathode materials for RMBs [141]. The pre-intercalated K ions not only enlarge the interchain spacing to facilitate diffusion of Mg ions, but also act as pillars to enhance the structural stability. Consequently, the $K_{0.2}VS_4$/N-TG composite exhibits a good rate capability of 113 mAh/g at 500 mA/g and excellent stability for 2000 cycles without obvious capacity decay. Besides, the polyvinylpyrrolidone (PVP) intercalated VS_4 also exhibits enhanced rate performance and cycling stability [142].

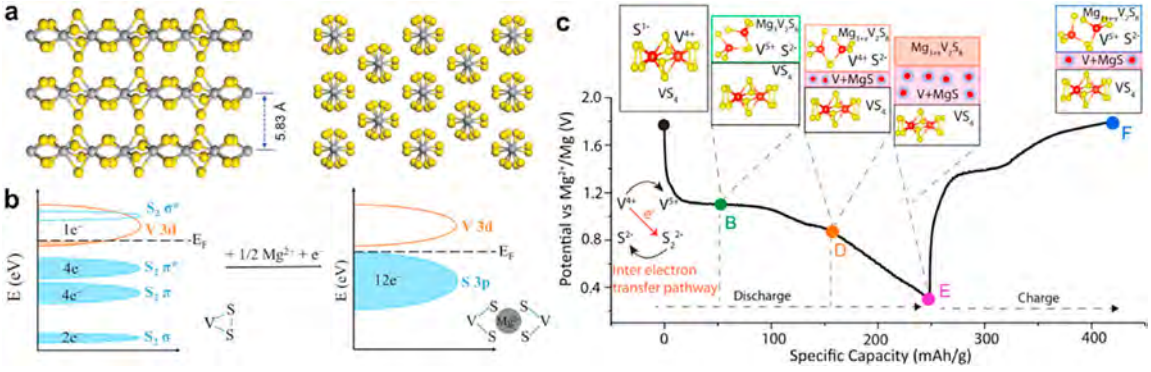

Fig. 9. VS_4 as cathode materials for RMBs. (a) Crystal structure of VS_4 [132]. (b) Schematic of the band structure of VS_4 before and after intercalation of Mg ions [133]. (c) Schematic illustration of the magnesium storage mechanism of VS_4 and the corresponding charge/discharge curves in the $Mg(AlCl_2EtBu)_2$/THF electrolyte with Mg metal as the anode [134].

Different from vanadium oxides and vanadates, vanadium chalcogenides are compatible with APC-based electrolytes with high magnesium plating/stripping efficiency. Various strategies have been proposed to improve the magnesium storage characteristics of vanadium chalcogenides, for example, nanocomposite construction, interlayer/interchain regulation, and defect engineering. The modified vanadium chalcogenides show high capacities of more than 200 mAh/g and good stability for over 1000 cycles. However, the working voltage of vanadium chalcogenides is below 1.5 V (*vs.* Mg^{2+}/Mg) thus limiting the energy density and making them not favorable in practical applications. Nevertheless, energy densities larger than 300 Wh/kg have been observed from VS_4-based cathodes due to the high capacity. It is larger than the theoretical energy density of Chevrel phase Mo_6S_8 (135 Wh/kg) [18] that is the typical cathode material in RMBs.

5. Vanadium-based phosphates

Vanadium-based phosphates such as $Li_3V_2(PO_4)_3$ (A = Li or Na), $Na_3V_2(PO_4)_2F_3$, and $Na_3(VO)_2(PO_4)_2F$ are promising cathode materials for LIBs and SIBs due to merits such as the high voltage, excellent structural stability, and open ion diffusion channels. Recently, the feasibility of vanadium-based phosphates as cathode materials in RMBs has been explored.

5.1. $A_xV_2(PO_4)_3$ (A = Li or Na)

$A_xV_2(PO_4)_3$ (A = Li or Na) has the Na^+ superionic conductor (NASICON) structure and an open framework for better ion intercalation and diffusion. Huang and coworkers have investigated the electrochemical properties of $Li_3V_2(PO_4)_3$ in 0.5 M Mg $(TFSI)_2$/AN [143]. The $Li_3V_2(PO_4)_3$/C composite exhibits a high discharging capacity of 197 mAh/g at 0.05C (1 C = 197 mA/g) and 55 °C. However, the capacity is not entirely contributed by Mg intercalation and re-intercalation of Li ions extracted from $Li_3V_2(PO_4)_3$ also contributes to the capacity. To avoid the influence of Li ions, fully delithiated $Li_3V_2(PO_4)_3$ ($V_2(PO_4)_3$) is assembled in a three-electrode cell. At 0.05C (1 C = 197 mAh/g) and 55 °C, a discharging capacity of 197 mAh/g is observed in the 5th cycle, but the cycling stability and rate performance are not discussed. Li et al. have reported that $Li_3V_2(PO_4)_3$/rGO delivers excellent electrochemical performance in 0.5 M $Mg(ClO_4)_2$/PC based on co-intercalation of Mg and Li ions [144]. $Li_3V_2(PO_4)_3$/rGO shows a reversible capacity of 124 mAh/g at 100 mA/g, capacity of 61 mAh/g at 1000 mA/g, and capacity retention of 80% after 300 cycles at 500 mA/g. The discharged product after 10 cycles is $Li_{1.86}Mg_{0.54}V_2(PO_4)_3$ thereby confirming the Li/Mg co-intercalation mechanism. Wang et al. have reported that $Li_3V_2(PO_4)_3$/C has good electrochemical properties in the 4 m Mg $(TFSI)_2$ aqueous electrolyte [145]. A capacity of 89.6 mAh/g is observed after 1000 cycles at 100 mA/g and a capacity of 72.8 mAh/g is still achieved at 3 A/g. The full aqueous Mg-ion battery comprising the $Mg_xLiV_2(PO_4)_3$ cathode shows outstanding cycling stability such as capacity retention of 92% after 6000 cycles at 2 A/g. However, the $Li_3V_2(PO_4)_3$/C composite has a smaller capacity of 20 mAh/g in the APC electrolyte with Mg being the anode [146].

$Na_3V_2(PO_4)_3$ is another candidate as cathode materials for RMBs (Fig. 10a). Cabello et al. have studied the electrochemical properties of $Na_3V_2(PO_4)_3$ in 0.5 M Mg $(TFSI)_2$/DME with Mg metal being the reference electrode [148]. At 10 mA/g, $Na_3V_2(PO_4)_3$ shows an initial discharging capacity of over 100 mAh/g with two plateaus at 1.6 V and 1.2 V (Fig. 10b) corresponding to intercalation of Na and Mg ions, respectively. The working voltage is less than the expected value due to the potential shift of Mg as the reference electrode in such electrolyte [151]. During cycling, the plateau at 1.6 V becomes narrower and that at 1.2 V is wider. After 140 cycles, the capacity is 60 mAh/g. The magnesium storage mechanism of desodiated $Na_3V_2(PO_4)_3$ ($Na_{1.3}V_2(PO_4)_3$) is a two-phase reaction between $Na_{1.3}V_2(PO_4)_3$ and $Mg_{0.8}Na_{1.3}V_2(PO_4)_3$. Zeng et al. have synthesized the mesoporous $Na_3V_2(PO_4)_3$/C composite and investigated the electrochemical properties in 0.3 M Mg $(TFSI)_2$/AN after electrochemical desodiation [149]. The desodiated mesoporous $Na_3V_2(PO_4)_3$/C ($Na_{1.12}V_2(PO_4)_3$/C) composite exhibits an initial discharging capacity of 88.8 mAh/g at 20 mA/g (Fig. 10c). It increases to 95.3 mAh/g in the second cycle and remains at 77 mAh/g after 100 cycles. The average discharge voltage of $Na_{1.12}V_2(PO_4)_3$/C is 2.5 V (*vs.* Mg^{2+}/Mg) and the discharged and charged products of $Na_{1.12}V_2(PO_4)_3$ are $Mg_{0.79}Na_{1.02}V_2(PO_4)_3$ and $Mg_{0.04}Na_{1.08}V_2(PO_4)_3$, respectively, indicative of reversible Mg intercalation/deintercalation. *Ex situ* XPS demonstrates that the charging/discharging process accompanies the redox process of $V^{3+} \leftrightarrow V^{4+}$. The intercalated Mg ions trend to occupy the 18e sites of desodiated $Na_3V_2(PO_4)_3$ and the volume change is 6.2% after intercalation of 0.75 Mg per formula (Fig. 10d and e) [148,150]. Aragón et al. have shown that the $NaV_2(PO_4)_3$/C composite obtained from $Na_3V_2(PO_4)_3$/C by chemical desodiation has a capacity of over 100 mAh/g in 0.1 M Mg $(TFSI)_2$/AN [152]. In addition, desodiated $Na_3V_2(PO_4)_3$/C also has a capacity of over 100 mAh/g in $Mg(BF_4)_2$/DME [147]. However, these electrolytes are incompatible with Mg anodes. Desodiated $Na_3V_2(PO_4)_3$/C shows a small capacity of 7 mAh/g in 0.2 M $[Mg_2(\mu\text{-}Cl)_2][AlCl_4]_2$/DME which is compatible with Mg anodes [153]. Therefore, identifying electrolytes that are compatible with both the $Na_3V_2(PO_4)_3$ cathode and Mg anode is crucial to further development of $Na_3V_2(PO_4)_3$ as cathodes. However, neither delithiated $Li_3V_2(PO_4)_3$ nor desodiated $Na_3V_2(PO_4)_3$ can be synthesized directly by conventional methods consequently hampering practical applications. One possible solution is to synthesize $Mg_{1.5}V_2(PO_4)_3$. Although $Mg_{1.5}V_2(PO_4)_3$ has not been reported, recently reported $Zn_3V_4(PO_4)_6$ ($Zn_{1.5}V_2(PO_4)_3$) [154] suggests that synthesis of $Mg_{1.5}V_2(PO_4)_3$ is possible because Zn and Mg ions have the same charge and similar radii.

5.2. $VOPO_4{\cdot}2H_2O$

$VOPO_4{\cdot}2H_2O$ has a layered structure with a large interlayer spacing of 7.41 Å, making it promising in metal-ion batteries. Ji et al. have investigated the effects of structural water and electrolytic water on the electrochemical properties of $VOPO_4{\cdot}2H_2O$ in the $Mg(ClO_4)_2$/PC electrolyte [155]. $VOPO_4{\cdot}2H_2O$ shows an initial capacity of 89 mAh/g in the wet electrolyte (0.1 M $Mg(ClO_4)_2{\cdot}6H_2O$/PC) and it is higher than that of $VOPO_4{\cdot}2H_2O$ in the dry electrolyte (0.1 M $Mg(ClO_4)_2$/PC) (11.2 mAh/g), $VOPO_4$ in the wet electrolyte (13.8 mAh/g), and $VOPO_4$ in the dry electrolyte (8.0 mAh/g) (Fig. 11a). Meanwhile, $VOPO_4{\cdot}2H_2O$ in the wet electrolyte exhibits a higher open circuit voltage (OCV) and lower voltage hysteresis (Fig. 11b). The high capacity of $VOPO_4{\cdot}2H_2O$ in the wet electrolyte is ascribed to the synergistic effects of electrolytic water and structural water (Fig. 11c). Electrolytic water can co-intercalate with Mg ions by partial desolvation which facilitates Mg intercalation, whereas structural water facilitates Mg diffusion in the interlayer by the shielding effect. To improve magnesium storage in $VOPO_4{\cdot}2H_2O$, Zhou et al. have expanded the interlayer spacing to 1.42 nm by replacing interlayered water with phenylamine (Fig. 11d) [28]. In the 0.25 M APC/THF electrolyte with Mg metal as the anode, phenylamine-intercalated $VOPO_4$ (PA-$VOPO_4$) shows capacities of 310 mAh/g at 50 mA/g and 109 mAh/g at 2000 mA/g, which is much higher than that of pristine $VOPO_4{\cdot}2H_2O$ (40 mAh/

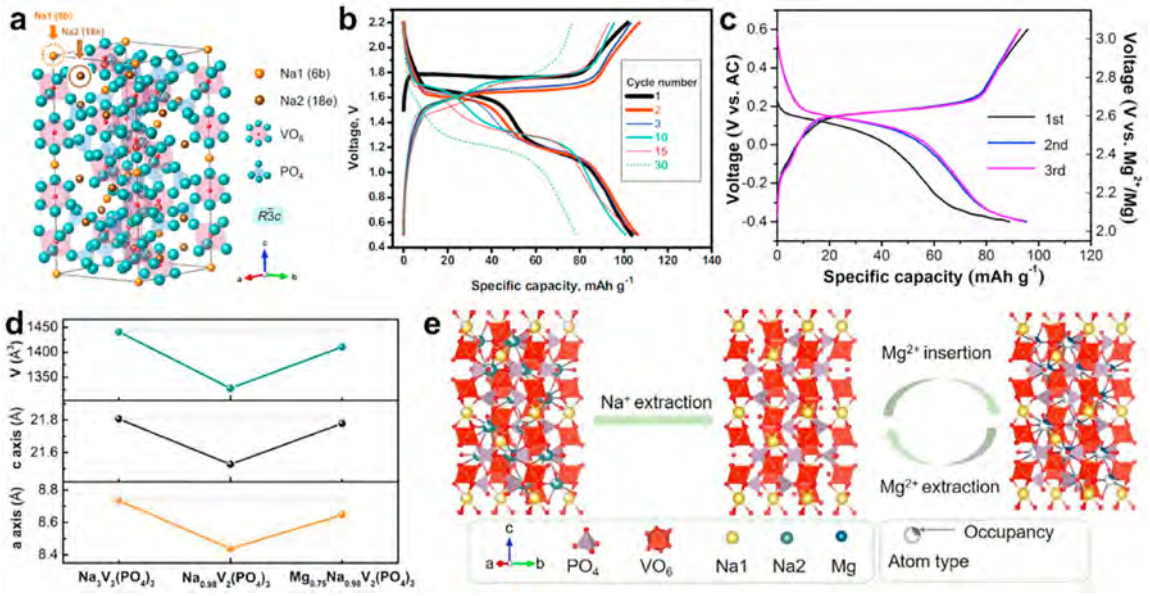

Fig. 10. $Na_xV_2(PO_4)_3$-based phosphates for RMBs. (a) Crystal structure of $Na_3V_2(PO_4)_3$ [147]. (b) Charging/discharging curves of $Na_3V_2(PO_4)_3$ at 10 mA/g in 0.5 M Mg $(TFSI)_2$/DME with Mg metal being the anode [148]. (c) Charging/discharging curves of the desodiated mesoporous $Na_3V_2(PO_4)_3$/C composite in 0.3 M Mg $(TFSI)_2$/AN with AC as the anode at 20 mA/g [149]. (d) Lattice parameters and unit cell volume of $Na_3V_2(PO_4)_3$, desodiated $Na_3V_2(PO_4)_3$ ($Na_{0.98}V_2(PO_4)_3$), and desodiated $Na_3V_2(PO_4)_3$ after Mg intercalation ($Mg_{0.75}Na_{0.98}V_2(PO_4)_3$). (e) Schematic of the structural change of $Na_3V_2(PO_4)_3$ during desodiation and subsequent Mg intercalation/deintercalation [150].

g). After 500 cycles at 100 mA/g, the capacity of PA-$VOPO_4$ is 192 mAh/g. The intercalated species in PA-$VOPO_4$ are $MgCl^+$ rather than Mg^{2+} and DFT calculation indicates that the diffusion barrier of $MgCl^+$ in PA-$VOPO_4$ is lower than that of Mg^{2+} (Fig. 11f). The fast kinetics of $MgCl^+$ in PA-$VOPO_4$ is responsible for the excellent rate performance. Notably, the discharge plateau of PA-$VOPO_4$ is located at about 1.0 V (vs. Mg^{2+}/Mg), which is lower than that of $VOPO_4 \cdot 2H_2O$ as reported by Ji et al. [155] and the expected value. The reason is unclear and needs more study.

5.3. Other vanadium-based phosphates

In addition to the aforementioned vanadium-based phosphates, some vanadium-based fluorophosphates are promising cathode

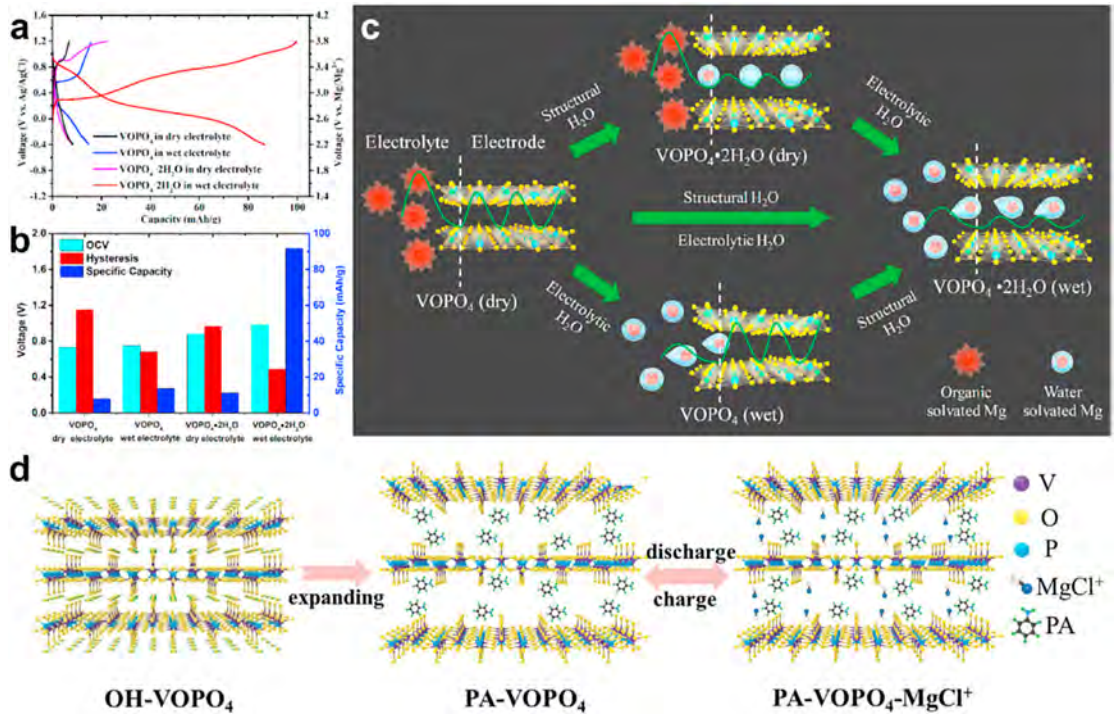

Fig. 11. Layered $VOPO_4 \cdot nH_2O$ as cathode materials for RMBs. (a) Charging/discharging curves of $VOPO_4$ and $VOPO_4 \cdot 2H_2O$ in dry and wet 0.1 M $Mg(ClO_4)_2$/PC electrolyte at 5 mA/g in the three-electrode system with carbon as the counter electrode and Ag/AgCl as the reference electrode, and (b) Corresponding OCV, voltage hysteresis and specific capacity. (c) Schematic illustration for the role of electrolytic and structural water on Mg storage of $VOPO_4 \cdot nH_2O$ [155]. (d) Schematic illustration of the formation and reaction mechanism of PA-$VOPO_4$ as RMBs cathode materials [28].

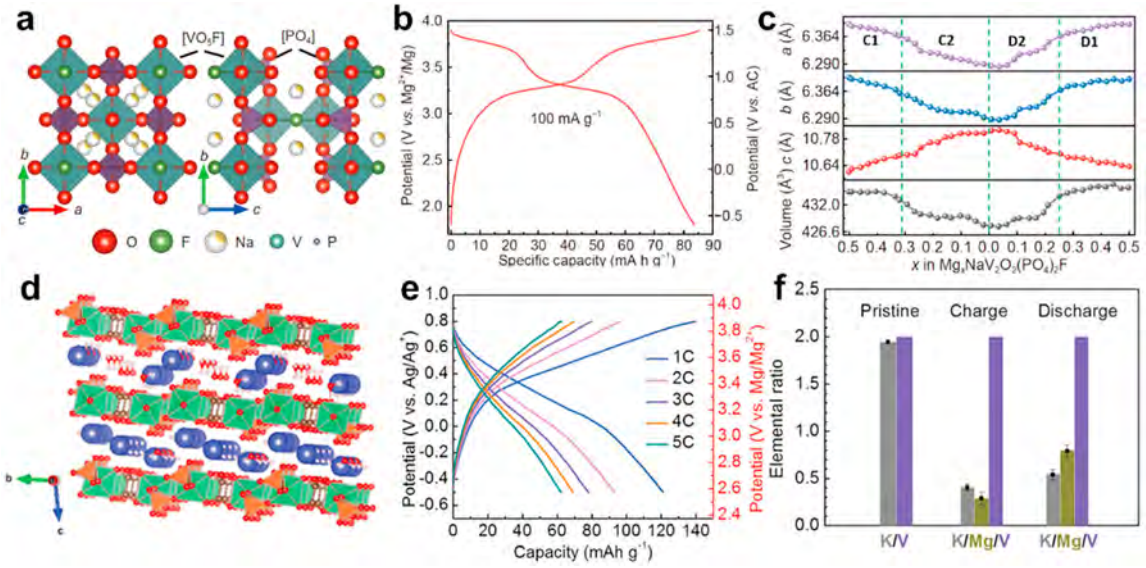

Fig. 12. Other vanadium-based phosphates for RMBs. (a) Crystal structure of $NaV_2O_2(PO_4)_2F$. (b) Charging/discharging curves of $NaV_2O_2(PO_4)_2F$/rGO in the 0.3 M Mg $(TFSI)_2$/AN electrolyte with AC as the anode. (c) Changes of the cell parameters of $NaV_2O_2(PO_4)_2F$ during the intercalation/deintercalation of Mg ions [27]. (d) Crystal structure of KVPCH, and (e) charging/discharging curves of KVPCH in the 0.1 M $Mg(ClO_4)_2$/PC electrolyte with AC as the counter electrode and Ag as the reference electrode. (f) Elemental ratios of KVPCH in different charging/discharging states [157].

materials for RMBs. Wang et al. have studied $NaV_2O_2(PO_4)_2F$/rGO (desodiated $Na_3V_2O_2(PO_4)_2F$/rGO) as high-voltage cathode materials for RMBs (Fig. 12a) [27]. In 0.3 M Mg $(TFSI)_2$/AN electrolyte, $NaV_2O_2(PO_4)_2F$/rGO shows a reversible capacity of 83.4 mAh/g with an average working voltage of ~3.3 V (*vs.* Mg^{2+}/Mg) at 100 mA/g (Fig. 12b). At high current densities of 2 A/g and 5 A/g, the capacities are still 50.6 mAh/g and 30.3 mAh/g, respectively. $NaV_2O_2(PO_4)_2F$/rGO also has excellent cycling characteristics such as capacity retention of 76% after 9500 cycles at 500 mA/g. The magnesium storage mechanism of $NaV_2O_2(PO_4)_2F$ is single-phase intercalation/deintercalation with a volume change of only 1.79% (Fig. 12c). Rubio et al. have reported that the desodiated $Na_5V(PO_4)_2F_2$ ($Na_3V(PO_4)_2F_2$) has a capacity of 136 mAh/g based on the multi-electron reaction of the V^{5+}/V^{4+} and V^{4+}/V^{3+} redox couples in the 0.5 M Mg $(TFSI)_2$ + 0.4 M H_2O/DME electrolyte with Mg as the anode [156]. However, large voltage hysteresis is observed and the average voltage is less than the calculated value.

Li et al. have reported $K_2(VO)_2(HPO_4)_2(C_2O_4)\cdot 4.5H_2O$ (KVPCH) with the layered structure (Fig. 12d) as cathode materials in RMBs [157]. In the 0.1 M $Mg(ClO_4)_2$/PC electrolyte, KVPCH has a capacity of 121 mAh/g at 1 C (109 mA/g) with an average working voltage of 3.2 V (*vs.* Mg^{2+}/Mg) based on the V^{5+}/V^{4+} redox couple (Fig. 12e). After 1500 cycles at 5 C, the capacity of KVPCH remains at 87% of the maximum capacity. Co-intercalation of K and Mg ions in KVPCH is revealed and the capacity is mainly contributed by Mg intercalation (Fig. 12f). Dongmo et al. have reported that $Na_3V_4(P_2O_7)_4(PO_4)$ (desodiated $Na_7V_4(P_2O_7)_4(PO_4)$) shows a high discharge plateau at ~3.45 V (*vs.* Mg^{2+}/Mg) in the 0.5 M $Mg(ClO_4)_2$/AN electrolyte [158].

Some amorphous vanadium-based phosphates have been employed as cathodes in RMBs. Arthur et al. have synthesized amorphous V_2O_5—P_2O_5 with different V_2O_5/P_2O_5 ratios [143]. In the $Mg(ClO_4)_2$/AN electrolyte with Mg being the anode, amorphous V_2O_5—P_2O_5 (75 : 25) exhibits the highest capacity of 121 mAh/g but the capacity decays rapidly to 57 mAh/g after 5 cycles. In addition, Wally et al. have prepared Na_2S—V_2O_5—P_2O_5 glass-ceramic nanocomposites but they have relatively poor electrochemical properties [159].

Compared to vanadium oxides, vanadates, and vanadium chalcogenides, vanadium-based phosphates usually have higher working voltages of over 2.5 V (*vs.* Mg^{2+}/Mg) due to the inductive effect of phosphate groups. For example, $NaV_2O_2(PO_4)_2F$/rGO has a working voltage of 3.3 V and long lifetime of 9500 cycles. However, the capacity of vanadium-based phosphates is limited due to the large mass of phosphate. Nonetheless, larger capacities can be obtained by taking advantage of the multi-electron reaction of vanadium, although this task is still challenging. Better vanadium-based phosphate cathode materials may be obtained by optimal composition design, phase regulation, and defect engineering in the future. In addition, it is necessary to identify the suitable electrolytes that are compatible with both Mg metal anodes and vanadium-based phosphates.

6. Optimization strategies for vanadium-based cathode materials for RMBs

In order to obtain better vanadium-based cathode materials for RMBs, various optimization strategies have been employed to improve magnesium storage. Optimization strategies that have been proposed mainly include the following.

(1) Nanostructure design - The sluggish solid-state diffusion kinetics of divalent Mg ions is one of the major obstacles for vanadium-based RMBs cathode materials to have good electrochemical properties. The problems are the large voltage hysteresis, poor rate performance, and low magnesium storage capacity. The proper nanostructure can shorten the diffusion distance and increase the specific surface area. It is noted that almost all previously reported high-performance vanadium-based cathode materials are nanostructured.

(2) Composite construction - Most vanadium-based cathode materials for RMBs, especially vanadium-based phosphates, suffer from poor electrical conductivity. In this case, combining vanadium-based materials and carbonaceous

Table 1
Electrochemical properties of vanadium-based cathode materials for RMBs.

Categories	Materials	Electrolytes	CE/RE	Voltage range (V vs. Mg^{2+}/Mg)	Capacity (mAh/g)/current density (mA/g)	Cycle number/capacity retention/ current density (mA/g)	Ref.
Vanadium oxide	V_2O_5	1 M $Mg(ClO_4)_2$/DMSO	Li/Li	1.9–2.9	~140/- (150 °C)	–	[36]
Vanadium oxide	V_2O_5	1 M $Mg(ClO_4)_2$/THF	Mg/Mg	–	194/-	–	[38]
Vanadium oxide	V_2O_5	1 M $Mg(ClO_4)_2$ + 1 M H_2O/AN	Mg/Ag	0.6–2.5	~170/-	20/~30%/-	[39]
Vanadium oxide	V_2O_5 nanocrystals	0.5 M $Mg(ClO_4)_2$/PC	AC/Ag	1.9–3.4	~180/7.6	–	[52]
Vanadium oxide	V_2O_5	0.1 M $Mg(ClO_4)_2$ + 1.79 M H_2O/PC	Mg/Mg	0.7–1.6	158.6/	9/~32%/-	[40]
Vanadium oxide	V_2O_5 thin-film	0.5 M $Mg(ClO_4)_2$/AN	-/Pt	2.0–3.15	~180/-	34/~83%/-	[23]
Vanadium oxide	S-doped V_2O_5	0.3 M $Mg(ClO_4)_2$ + 1.8 M H_2O/PC	Pt/Mg	0.9–2.4	~300/60	–	[42]
Vanadium oxide	MnO_2/S-doped V_2O_5	0.3 M $Mg(ClO_4)_2$ + 1.8 M H_2O/PC	Pt/Mg	0.9–2.4	~420/60	–	[42]
Vanadium oxide	V_2O_5	1 M Mg $(TFSI)_2$/G2 with 2600 ppm H_2O	AC/AC	0.6–4.2	~260/-	–	[41]
Vanadium oxide	V_2O_5	0.5 M Mg $(TFSI)_2$/$PY_{14}TFSI$	AC/AC	1.3–3.5	295/15, ~275/30, ~250/60, ~215/150, ~180/300, ~150/600, ~110/1500 (110 °C)	50/76%/150 (110 °C)	[49]
Vanadium oxide	Flower-like V_2O_5 microspheres	0.25 M $Mg(AlCl_2EtBu)_2$/THF	Mg/Mg	0.1–2.0	126.2/50, 92/100, 80/150, 62/200	80/71.9%/50	[54]
Vanadium oxide	V_2O_5 nanospheres	0.2 M $Mg(ClO_4)_2$/AN	AC/AC	1.6–2.6	~225/10, ~100/30, ~60/50, ~40/80	100/~46%/50	[53]
Vanadium oxide	V_2O_5–TiO_2 nanocomposite	0.5 M Mg $(TFSI)_2$/$PY_{14}TFSI$	AC/AC	~0.9–3.3	~310/15 (110 °C)	20/>100%/15 (110 °C)	[57]
Vanadium oxide	GO/V_2O_5 composites	0.25 M $Mg(AlCl_2EtBu)_2$/THF	Mg/Mg	1.0–2.8	178/-	20/~78.7%/-	[55]
Vanadium oxide	V_2O_5/graphene	$MgNO_3 \cdot 6H_2O$/succinonitrile + TEGDME	Mg/Mg	0.5–1.6	~86/-	–	[56]
Vanadium oxide	Ti–V_2O_{5-x}	0.5 M $Mg(ClO_4)_2$/AN	AC/AC	1.75–3.35	245.4/100, 205.8/200, 174.8/300, 157.0/400, 148.0/500	400/~81%/100	[58]
Vanadium oxide	PEDOT intercalated V_2O_5	0.4 M $(PhMgCl)_2$-$AlCl_3$/THF with CTAB additive	Mg/Mg	0.01–2.3	288.7/50, ~230/100, 153.8/300, 110.7/500	500/~65%/500	[62]
Vanadium oxide	β-V_2O_5	0.1 M $Mg(ClO_4)_2$/AN	AC/AC	0.1–3.6	~450/23.5	15/>100%/23.5	[65]
Vanadium oxide	ζ-V_2O_5 nanowires	0.2 M Mg $(TFSI)_2$/PC	AC/AC	0.2–3.4	~140/6 (50 °C)	100/~65%/6 (50 °C)	[60]
Vanadium oxide	Nanoscale ζ-V_2O_5	0.5 M Mg $(TFSI)_2$/$PY_{14}TFSI$	AC/AC	~0.75–3.25	~130/15 (110 °C)	15/>100%/15 (110 °C)	[68]
Vanadium oxide	Amorphous V_2O_5	0.3 M Mg $(TFSI)_2$/glyme + DME	AC/AC	0.9–3.4	183/30	40/-/30	[70]
Vanadium oxide	Amorphous V_2O_5 thin-film	0.1 M $Mg(ClO_4)_2$ + 0.6 M H_2O/PC	AC/AC	1.6–3.0	~125/18, ~70/54, ~35/540, ~30/1,020, ~25/1800	90/~65%/18	[71]
Vanadium oxide	Amorphous V_2O_5 nanocluster/porous carbon	0.2 M $[Mg_2(\mu\text{-}Cl)_2(DME)_4][AlCl_4]_2$/DME	Mg/Mg	0.5–2.8	~225/40, ~180/80, ~140/160, ~120/320, ~100/640	100/~62.5%/320	[69]
Vanadium oxide	$V_2O_5 \cdot nH_2O$	1 M $Mg(ClO_4)_2$/AN	Mg/Ag	1.6–3.5	~170/-	–	[39]
		$MgCl_2/AlCl_3$/EMIC	Al/Al	1.7–3.2	~170/- (80 °C)		
Vanadium oxide	$V_2O_5 \cdot nH_2O$	0.3 M $Mg(ClO_4)_2$/PC	S–V_2O_5/Ag–AgCl	0.9–2.4	463/60	–	[77]
Vanadium oxide	S-doped $V_2O_5 \cdot nH_2O$	0.3 M $Mg(ClO_4)_2$ + 1.8 M H_2O/PC	Pt/Ag–AgCl	0.9–2.6	450/21	–	[78]
Vanadium oxide	$V_2O_5 \cdot nH_2O$/C composite[a]	1 M $Mg(ClO_4)_2$/AN	Mg/Ag	~2.0–3.5	~600/1	35/~66%/17	[73]
Vanadium oxide	$V_2O_5 \cdot 1.42H_2O$ nanowire/ graphene composite	0.3 M Mg $(TFSI)_2$/AN	AC/AC	1.6–3.4	~320/50, ~220/200, ~150/500, ~120/1,000, ~100/2000	200/81%/1000	[24]
Vanadium oxide	PEO intercalated $V_2O_5 \cdot nH_2O$	0.5 M $Mg(ClO_4)_2$/AN	C/Mg	1.0–3.0	125/10	35/~77%/10	[81]
Vanadium oxide	PANI intercalated $V_2O_5 \cdot nH_2O$	0.3 M Mg $(TFSI)_2$/AN	AC/AC	1.2–3.4	275/100, 250/200, 220/500, 175/1,000, 155/2,000, 130/4000	500/~70%/4000	[79]
Vanadium oxide	VO_2(B) nanorods	1 M $Mg(ClO_4)_2$/AN	C/Ag	1.65–2.95	391/25, 370/50, 341/100	60/41.9%/60	[89]
Vanadium oxide	$H_2V_3O_8$ nanowires	0.5 M $Mg(ClO_4)_2$/AN	AC/AC	1.2–3.1	304.2/50	20/85.9%/50	[83]
Vanadium oxide	$H_2V_3O_8$ nanowires	0.5 M $Mg(ClO_4)_2$/AN	AC/AC	1.1–3.6	231/10, 201/20, 170/40, 97/80 (60 °C)	100/77%/40 (60 °C)	[90]
Vanadium oxide	V_6O_{13} nanosheets	1 M $Mg(ClO_4)_2$/AN	Mg/Mg	0.3–2.3	324/20, 278/40, 244/60, 214/80	30/71.9%/40	[92]
Vanadium oxide	V_2O_3@rGO microspheres	0.3 M Mg $(TFSI)_2$/AN	AC/AC	1.4–3.9	291.3/50, 280.1/100, 259.1/200, 232.5/500, 210.4/1,000, 185.3/2000	1000/88.5%/500	[93]
Vanadium oxide	VO_x-NTs	0.25 M $Mg(AlBu_2Cl_2)_2$/THF	Mg/Mg	0.2–0.8	~75/5	–	[94]
Vanadium oxide	$Cu_{0.1}$-doped VO_x-NTs	0.25 M $Mg(AlBu_2Cl_2)_2$/THF	Mg/Mg	0.2–0.9	120.2/10	–	[96]
Vanadium oxide	HT-VO_x	0.5 M $Mg(ClO_4)_2$/AN	AZ31 Mg alloy/Ag	1.5–3.4	218/60	20/70.8%/60	[97]
Vanadium oxide	C_{12}-VO_x-NTs	1 M $Mg(ClO_4)_2$/AN	Mg/Mg	0.2–3.2	146 ± 35/5	10/15%/5	[98]

Vanadate	$NaV_3O_8 \cdot (H_2O)_y$	0.5 M $Mg(ClO_4)_2$/PC 1 M $Mg(ClO_4)_2$ + 2 M H_2O/AN	Mg/Ag –	1.6–3.6 –	80/10 210/-	26/~20%/10 –	[99]
Vanadate	$NaV_3O_8 \cdot 1.69H_2O$ nanobelts	0.4 M $(PhMgCl)_2$-$AlCl_3$/THF	Mg/Mg	0.05–2.0	~110/10, ~50/20, ~35/50, ~25/100, ~15/200, ~7/500	100/~80%/50	[100]
Vanadate	$Na_2V_6O_{16} \cdot 1.63H_2O$ nanowires	0.5 M Mg $(TFSI)_2$/DME	AC/AC	1.4–3.7	228/20, 193/30, 145/50, 105/80, 91/100, ~50/200, ~30/500	450/71%/200	[101]
Vanadate	$NaV_8O_{20} \cdot nH_2O$ nanobelts	1 M $Mg(ClO_4)_2$/TEGDME-H_2O (v/v = 4/1)	Pt/Ag–AgCl	1.9–3.8	350.6/300, 264.3/500, 211.0/800, 185.5/1,000, 155.6/1,500, 126.3/2,000, 110.1/2,500, 94.3/3000	1000/~50%/1500	[102]
Vanadate	NaV_3O_8	0.5 M $Mg(ClO_4)_2$/AN	AC/AC	1.4–3.1	260/50, 184/100, 123.9/200, 86.6/500, 62.4/1000	100/88.3%/500	[103]
Vanadate	NaV_6O_{15}	1 M $Mg(ClO_4)_2$/AN	Mg/Mg	0.1–2.3	~230/-	50/~20%/-	[104]
Vanadate	NaV_6O_{15}	0.5 M $Mg(ClO_4)_2$/AN	AC/AC	1.65–2.95	210.1/10, 137.0/20, 111.7/50, 80.2/100, 52.3/200, 27.2/500	95/~95%/20	[105]
Vanadate	$Na_{0.4}V_{1.25}Ti_{0.75}O_4$	0.5 M $Mg(CB_{11}H_{12})_2$/tetraglyme	Mg/Mg	0.1–3.0	~80/5 (60 °C)	–	[107]
Vanadate	$Mg(V_3O_8)_2 \cdot (H_2O)_y$	$MgCl_2$/$AlCl_3$/EMIC	Mg/Al	1.3–2.5	150/- (80 °C)	60/~40%/- (80 °C)	[99]
Vanadate	$Mg_{0.1}V_2O_5 \cdot 1.8H_2O$	0.5 M $Mg(ClO_4)_2$/AN	Pt/Ag	1.7–3.7	300/30	7/93.3%/30	[108]
Vanadate	$Mg_{0.1}V_2O_5 \cdot 2.35H_2O$	0.5 M Mg $(TFSI)_2$ + 0.5 M dipro-glyme/AN	C/Ag	2.1–3.9	143/-	10/>100%/-	[109]
Vanadate	$Mg_{0.3}V_2O_5 \cdot 1.1H_2O$ nanowires	0.3 M Mg $(TFSI)_2$/AN	AC/AC	1.4–3.4	162/100, 145/200, 134/500, 120/1,000, 85/2,000, 50/4000	500/>100%/100, 10,000/>100%/1,000, 10,000/80%/2000	[110]
Vanadate	MgV_2O_6	$Mg(AlBu_2Cl_2)_2$/THF	Mg/Mg	0.2–2.1	120/-	15/~25%/-	[160]
Vanadate	MgV_2O_6	1 M $Mg(ClO_4)_2$/AN	Mg/Mg	0.0–2.0	120/-	10/~33.3%/-	[161]
Vanadate	$Mg(Mg_{0.5}V_{1.4}Ni_{0.1})O_4$	1 M Mg $(TFSI)_2$/triglyme	AZ31 Mg alloy/AZ31 Mg alloy	~1.35–2.85	66/5 (90 °C)	19/>100%/5 (90 °C)	[115]
Vanadate	MgV_2O_4 nanocrystals	0.5 M Mg $(TFSI)_2$/$PY_{14}TFSI$	AC/AC	0.6–3.5 0.9–3.4	~235/- (110 °C) ~175/- (110 °C)	–	[49]
Vanadate	$Mg(Mg_{0.5}V_{1.5})O_4$ hierarchical microspheres	0.3 M Mg $(TFSI)_2$/AN	AC/AC	1.4–3.9	250/100, 223/200, 201/500, 184/1,000, 165/2,000, 142/4000	100/92.1%/100, 1000/~70%/4000	[113]
Vanadate	$Mo_{2.48}VO_{9.93}$	0.5 M Mg $(TFSI)_2$/AN	AC/AC	1.73–3.33	397/2	15/~60%/2	[116]
Vanadate	$FeVO_4$ nanorods	0.3 M Mg $(TFSI)_2$/AN	AC/AC	0.9–3.3	366/50, ~260/100, ~225/200, ~190/500, 165.1/1000 (50 °C)	100/74%/50, 1000/85%/1000 (50 °C)	[118]
Vanadate	FVO@CC	0.3 M Mg $(TFSI)_2$/AN	AC/AC	1.4–3.6	298/50, 277/100, 229/200, 178/500, 144/1,000, 120/2000	100/89%/100, 5000/~60%/2000	[119]
Vanadate	$Mn_{0.04}V_2O_5 \cdot 1.17H_2O$ nanobelts	0.3 M Mg $(TFSI)_2$/AN	AC/AC	1.4–3.4	145/50, 131/100, 110/200, 108/500, 97/1,000, 80/2,000, 60/3,000, 50/4000	10,000/82%/2000	[120]
Vanadate	$NH_4V_4O_{10}$	0.5 M $Mg(ClO_4)_2$/AN	AC/AC	1.87–3.47 1.97–3.07	174.8/42.1, ~130/105.3, ~110/210.6, 68.9/421.2 101/210.6.	100/~20%/210.6, 100/>100%/210.6	[121]
Vanadate	$(NH_4)_2V_6O_{16} \cdot 1.5H_2O$ nanobelts	0.5 M $Mg(ClO_4)_2$/AN	AC/AC	2.0–3.1 V	123/50, 110/100, 95/200, 73/500, 56/1000	50/63%/50	[122]
Vanadate	$H_{11}Al_2V_6O_{23.2}$ microspheres	0.3 M Mg $(TFSI)_2$/AN	AC/AC	1.4–3.5	165/100, 127/200, 98/500, 75/1,000, 60/2,000, 47/4000	50/98%/50, 3000/87%/1000	[123]
Vanadium chalcogenide	2-EHA intercalated VS_2 nanoflowers	$Mg(HMDS)_2$-4$MgCl_2$/2THF-$PP_{14}TFSI$	Mg/Mg	0.2–2.2	249/100, 212/300, 179/500, 140/1,000, 102/2000	100/78%/100, 600/~70%/1000	[125]
Vanadium chalcogenide	Expanded VS_2 nanosheets assemblies	0.4 M $(PhMgCl)_2$-$AlCl_3$/THF	Mg/Mg	0.25–2.0	237/100, 222/200, 208/400, 189/800, 179/1,000, 147/2000	200/94.9%/100, 1000/86%/1000	[126]
Vanadium chalcogenide	VS_2 nanosheets	0.4 M $(PhMgCl)_2$-$AlCl_3$ + 0.2 M $PP_{14}Cl$/THF	Mg/Mg	0.01–2.0	299/50, 299/100, 292/200, 280/500, 257/1,000, 214/2000	68/~98%/200, 300/~70%/1000	[128]
Vanadium chalcogenide	VSe_2	0.25 M $Mg(AlCl_2EtBu)_2$/THF	Mg/Mg	0.2–1.8	122/10	60/~90%/10	[129]
Vanadium chalcogenide	VSe_2	$(PhMgCl)_2$-$AlCl_3$/THF	Mg/Mg	0.5–2.0	~130/5	40/~66%/5	[124]
Vanadium chalcogenide	VSe_2 hierarchical rods	0.2 M $Mg(HMDS)_2$-$MgCl_2$-2$AlCl_3$/THF	Mg/Mg	0.1–2.5	~350/50, 85/100, 74/200, 57/500	30/~28%/50	[130]
Vanadium chalcogenide	VSe_2 nanoparticles/rGO	0.25 M $(PhMgCl)_2$-$AlCl_3$/THF	Mg/Mg	0.2–1.7	235.5/50, 213.9/200, 175.5/500, 121.0/800, 97.8/1000	500/62.8%/50	[131]
Vanadium chalcogenide	VS_4 nanodendrites	0.4 M $(PhMgCl)_2$-$AlCl_3$/THF	Mg/Mg	0.2–2.2	137/50, 130/150, 123/300, 106/500	180/~85%/100, 800/71.6%/500	[132]
Vanadium chalcogenide	Flower-like VS_4 microspheres	0.4 M $(PhMgCl)_2$-$AlCl_3$/THF	Mg/Mg	0.2–2.2	95/10, 80/20, 75/50, 70/100, 65/200, 60/300	400/90%/50	[162]
Vanadium chalcogenide	VS_4@rGO	0.25 M $(PhMgCl)_2$-$AlCl_3$ + 0.25 M $PY_{14}Cl$/THF	Mg/Mg	0.2–2.0	268.3/50, 157.9/100, 132.8/200, 116.2/500, 101.4/1,000, 85.9/2000	100/~55%/50, 200/63.7%/500	[140]
Vanadium chalcogenide	VS_4/rGO	0.4 M Mg $[B(hfip)_4]_2$)/DME	Mg/Mg	0.01–2.5	440/50, ~320/100, ~220/200, 119/500	50/~50%/100	[133]

(continued on next page)

Table 1 (*continued*)

Categories	Materials	Electrolytes	CE/RE	Voltage range (V vs. Mg^{2+}/Mg)	Capacity (mAh/g)/current density (mA/g)	Cycle number/capacity retention/current density (mA/g)	Ref.
Vanadium chalcogenide	Core-shell CNT@VS_4	0.4 M $(PhMgCl)_2$-$AlCl_3$/THF	Mg/Mg	0.2–2.2	214.8/50, 170.4/100, 149.2/200, 124.6/500, 100.3/1,000, 77.2/2000	800/68%/500	[136]
Vanadium chalcogenide	VS_4@Ti_3C_2/C	0.25 M $(PhMgCl)_2$-$AlCl_3$/THF	Mg/Mg	0.01–2.0	492/50, 388/100, 285/200, 176/500, 129/1000	900/80%/500	[135]
Vanadium chalcogenide	3%Mo-doped VS_4 hollow microspheres	0.4 M $(PhMgCl)_2$-$AlCl_3$/THF	Mg/Mg	0.2–2.1	140/20, 125/30, 112/50, 101/100, 88/200, 80/300, 70/500	350/~99%/50, 350/~96%/500	[137]
Vanadium chalcogenide	Mo/O co-doped VS_4 hollow microspheres	0.4 M $(PhMgCl)_2$-$AlCl_3$/THF	Mg/Mg	0.2–2.1	144/50, 137.5/100, 121.1/200, 92.5/500, 75.2/1000	500/>100%/50, 1000/92%/1000	[138]
Vanadium chalcogenide	Mo-doped VS_4/N-TG	0.4 M $(PhMgCl)_2$-$AlCl_3$/THF	Mg/Mg	0.2–2.1	151.7/20, 136.8/30, 124.3/50, 113/100, 99/200, 89.5/300, 76.6/500	600/>100%/50, 1200/80.6%/500	[139]
Vanadium chalcogenide	$K_{0.2}VS_4$/N-TG	0.4 M $(PhMgCl)_2$-$AlCl_3$/THF	Mg/Mg	0.2–2.1	188.6/50, 174.9/80, 155.8/100, 144.0/200, 124.9/300, 113.0/500, 98.6/1000	200/>100%/50, 2000/~100%/1000	[141]
Vanadium chalcogenide	PVP-intercalated VS_4	0.4 M $(PhMgCl)_2$-$AlCl_3$/THF	Mg/Mg	0.2–2.1	140/50, 120/100, 108/200, 90/500, 73/1,000, 60/2,000, 45/5000	500/~100%/50, 1500/80%/5000	[142]
Vanadium-based phosphate	Amorphous V_2O_5–P_2O_5 (75 : 25)	1 M $Mg(ClO_4)_2$/AN	Mg/Ag	1.2–3.3	121/5	5/47%/5	[163]
V-based phosphate	$V_2(PO_4)_3$/C	0.5 M Mg $(TFSI)_2$/AN	Mg/Ag	1.5–3.9	197/~10 (55 °C)	–	[143]
Vanadium-based phosphate	$Li_3V_2(PO_4)_3$/rGO	0.5 M $Mg(ClO_4)_2$/PC	AC/Ag	2.04–3.84	124/100, 106/200, 85/500, 61/1000	300/80%/500	[144]
Vanadium-based phosphate	$Li_3V_2(PO_4)_3$/C	4 m Mg $(TFSI)_2/H_2O$	AC/Ag–AgCl	2.4–3.6	102/100, ~93/200, ~83/500, ~80/1,000, ~75/2,000, 72.8/3000	1000/88%/100	[145]
Vanadium-based phosphate	$Na_3V_2(PO_4)_3$/C	0.5 M Mg $(TFSI)_2$/DME	Mg/Mg	0.5–2.2	~110/10	140/~55%/10	[148]
Vanadium-based phosphate	Mesoporous $Na_{1.12}V_2(PO_4)_3$/C	0.3 M Mg $(TFSI)_2$/AN	AC/AC	2.05–3.05	95.3/20	100/81%/20	[149]
Vanadium-based phosphate	$NaV_2(PO_4)_3$/C	0.1 M Mg $(TFSI)_2$/AN	AC/AC	0.85–1.9	~110/~2, ~75/~5	–	[152]
Vanadium-based phosphate	$NaV_2(PO_4)_3$/C	0.3 M $Mg(BF_4)_2$ in EC/DEC (v/v = 1/1),	AC/Ag	1.5–3.5	103/5	20/~85%/5	[147]
Vanadium-based phosphate	honeycomb-like $NaV_2(PO_4)_3$/C/G	Mg $(TFSI)_2$/AN	AC/AC	2.05–3.05	87/10, 78/20	60/85%/20	[150]
Vanadium-based phosphate	$Na_3VCr(PO_4)_3$/C	0.5 M Mg $(TFSI)_2$ (16% H_2O)/DME 0.1 M Mg $(TFSI)_2$ (16% H_2O)/AN	Mg/Mg AC/AC	0.2–2.55 0.01–3.8	79.2/2 (−15 °C) ~82/20 (−15 °C)	20/~75%/2 (−15 °C) 23/~60/20 (−15 °C)	[164]
Vanadium-based phosphate	$VOPO_4 \cdot 2H_2O$	0.1 M $Mg(ClO_4)_2$ + 0.6 M H_2O/PC	C/Ag–AgCl	2.2–3.8	89/5	50/~80%/5	[155]
Vanadium-based phosphate	PA-$VOPO_4$ nanosheets	0.25 M $(PhMgCl)_2$-$AlCl_3$/THF	Mg/Mg	0.3–2.4	310/50, 275/100, 220/200, 175/500, 140/1,000, 109/2000	500/~70/500	[28]
Vanadium-based phosphate	$NaV_2O_2(PO_4)_2F$/rGO	0.3 M Mg $(TFSI)_2$/AN	AC/AC	1.8–3.9	97.2/20, 95.4/50, 90.8/100, 83.9/200, 70.9/500, 61.5/1,000, 50.6/2,000, 30.3/3000	9500/76%/500	[27]
Vanadium-based phosphate	$Na_3V(PO_4)_2F_2$	0.5 M Mg $(TFSI)_2$ + 0.4 M H_2O/DME	Mg/Mg	0.2–2.5	136/5	–	[156]
Vanadium-based phosphate	KVPCH	0.1 M $Mg(ClO_4)_2$/PC	AC/Ag	2.6–3.9	121/109, 93/218, 78/327, 69/436, 62/545	1500/87%/545	[157]
Vanadium-based phosphate	$NaV_2(PO_4)_3$/$Na_3V_4(P_2O_7)_4(PO_4)$/C	0.5 M $Mg(ClO_4)_2$/AN	AC/AC	1.47–3.865	53.3/2 (50 °C)	–	[158]

CE: counter electrode, RE: reference electrode.

[a] We believe that the unit of current density in the original paper is wrong, it should be mA/g instead of A/g.

materials with good conductivity to fabricate composites can improve the electronic conductivity and enhance magnesium storage performance. The proper composite structure can also prevent agglomeration of nanostructured vanadium-based materials and produce large electrode-electrolyte interfaces with high utilization of the active materials.

(3) Defect engineering - Defect engineering such as doping and vacancy introduction is another effective strategy to improve the electrical conductivity. The impurity energy levels in the bandgap generated by the suitable dopants can reduce the electron transition energy to improve the conductivity. Anionic vacancies can lead to partial reduction of vanadium by the charge compensation effect and mixed-valence vanadium shows better conductivity. Anionic vacancies also facilitate diffusion of Mg ions.

(4) Interlayer regulation - Many vanadium-based cathode materials possess the layered crystal structure but the relatively small interlayer spacing hinders intercalation and diffusion of Mg ions. Therefore, interlayer regulation, that is, introducing ions or molecules into interlayers, is an effective method to facilitate diffusion of Mg ions by enlarging the interlayer spacing. The added ions and molecules also act as pillars to stabilize the layered structure. Introducing cations into interlayers can produce mixed valence states of vanadium to improve the conductivity. Similarly, interchain regulation is an effective strategy to improve the magnesium storage properties of vanadium-based cathode materials with the chain-like crystal structure.

(5) Electrolyte regulation — Electrolytes affect the magnesium storage properties of vanadium-based materials. For example, many vanadium-based materials have excellent magnesium storage performance in Mg $(TFSI)_2$ or $Mg(ClO_4)_2$-based electrolytes but low storage in APC-based electrolytes. Adjusting the composition of electrolyte can change the solvation shell of Mg ions to regulate the Mg intercalation behavior in vanadium-based cathode materials, for instance, the desolvation energy. In addition, adding Li/Na salts to electrolytes change the intercalation species from divalent Mg ions to monovalent Li/Na-ion can improve the electrochemical kinetics of vanadium-based materials. However, such battery systems with electrolytes containing Li/Na salts are hybrid-ion batteries (Daniel type) rather than “real RMBs” (rocking-chair type) and therefore are not discussed in this review. Besides, cations of some electrolyte additives such as PP_{14}^{+} and CTA^{+} can be co-intercalated into vanadium-based materials during the first discharging step to accomplish interlayer/interchain regulation. All in all, different optimization strategies can be applied to the vanadium-based cathode materials at the same time to produce synergistic effects.

7. Conclusions and outlook

Vanadium-based materials constitute an important class of cathode materials for RMBs. Herein, we provide a comprehensive overview of vanadium-based cathode materials for RMBs including vanadium oxides, vanadates, vanadium chalcogenides, and vanadium-based phosphates. The structure, electrochemical properties, optimization strategies, structure—properties relationship, and reaction mechanisms of various vanadium-based cathode materials are described. In order to provide guidance to future research in this important area, both the virtues and shortcomings of the different materials are summarized here.

Vanadium oxides have a high capacity (over 300 mAh/g) and intermediate voltage (2.0—2.5 V *vs.* Mg^{2+}/Mg) but poor cycling stability (Table 1). In comparison, some vanadates have excellent cycling stability (over 1000 cycles) due to the pillar effect of cations at the interlayer as well as structural stability. Vanadium oxides and vanadates containing structural water usually exhibit better Mg diffusion kinetics stemming from the shielding effect rendered by water molecules which reduce the electrostatic interactions between Mg ions and host materials in addition to those among Mg ions. Some vanadium oxides and vanadates have excellent electrochemical characteristics in $Mg(ClO_4)_2$- or Mg $(TFSI)_2$-based electrolytes, but these electrolytes are usually incompatible with Mg metal anodes due to the passivation effect. Moreover, most vanadium oxides and vanadates deliver poor electrochemical performance in complex electrolytes because of efficient Mg plating and stripping. On the other hand, vanadium chalcogenides have high capacities and good cycling properties in some complex electrolytes that are compatible with Mg anodes, but their average working voltages are restricted (below 2.0 V *vs.* Mg^{2+}/Mg). Some vanadium-based phosphates can function at a high voltage of over 3.0 V (*vs.* Mg^{2+}/Mg) and exhibit excellent cycling stability (over 1000 cycles). However, the magnesium storage capacity of vanadium-based phosphates is typically less than 150 mAh/g and they are also incompatible with common complex electrolytes.

Although some high-performance vanadium-based cathode materials have been designed for RMBs, there are still shortcomings and challenges. For instance, most vanadium-based materials except vanadium chalcogenides have poor electrochemical properties in electrolytes that possess high Mg plating/stripping efficiency. Therefore, suitable electrolytes that are compatible with both vanadium-based materials and Mg anodes are critical to the development of RMBs. In this respect, constructing an artificial surface on Mg anodes can facilitate reversible Mg plating/stripping in $Mg(ClO_4)_2$- or Mg $(TFSI)_2$-based electrolytes to overcome one of the obstacles.

In spite of recent advances, the reaction mechanism of some vanadium-based materials is still unclear or even controversial, for example, whether the intercalated species are Mg ions or protons. Therefore, more in-depth investigations are required. The mass loading of vanadium-based cathode is typically less than 2 mg/cm^2 and does not meet practical requirements. In comparison with that the areal capacity of commercial LIBs is over 3.0 mAh/cm^2, the mass loading should exceed 10 mg/cm^2 if the vanadium-based cathode has a capacity of 300 mAh/g. However, the magnesium storage performance of vanadium-based materials with high mass loadings is not well studied. Prior to commercial adoption, large-scale synthesis of high-performance vanadium-based cathode materials must be demonstrated and this is certainly one of the future research directions. In summary, although vanadium-based cathode materials have large potential in RMBs, more work must be done to enrich our understanding and bring the technology to fruition.

Author contribution

All authors contribute to the literature search and writing of the review. FY Xiong and PK Chu are the lead writers.

Declaration of competing interest

The authors declare that they have no known competing financial interests or personal relationships that could have appeared to influence the work reported in this paper.

Data availability

No data was used for the research described in the article.

Acknowledgements

The work was supported by City University of Hong Kong Strategic Research Grant (SRG) (No. 7005505), City University of Hong Kong Donation Research Grant (DON-RMG No. 9229021), as well as Hong Kong Scholars Program (No. XJ2021021).

References

[1] D. Larcher, J.M. Tarascon, Towards greener and more sustainable batteries for electrical energy storage, Nat. Chem. 7 (2015) 19–29, https://doi.org/10.1038/nchem.2085.
[2] J.B. Goodenough, Electrochemical energy storage in a sustainable modern society, Energy Environ. Sci. 7 (2014) 14–18, https://doi.org/10.1039/c3ee42613k.
[3] Z. Yang, J. Zhang, M.C. Kintner-Meyer, X. Lu, D. Choi, J.P. Lemmon, J. Liu, Electrochemical energy storage for green grid, Chem. Rev. 111 (2011) 3577–3613, https://doi.org/10.1021/cr100290v.
[4] Y. Fang, Z. Chen, L. Xiao, X. Ai, Y. Cao, H. Yang, Recent progress in iron-based electrode materials for grid-scale sodium-ion batteries, Small 14 (2018), 1703116, https://doi.org/10.1002/smll.201703116.
[5] Z. Yao, Q. Wu, K. Chen, J. Liu, C. Li, Shallow-layer pillaring of a conductive polymer in monolithic grains to drive superior zinc storage via a cascading effect, Energy Environ. Sci. 13 (2020) 3149–3163, https://doi.org/10.1039/d0ee01531h.
[6] F. Xiong, S. Tan, X. Yao, Q. An, L. Mai, Crystal defect modulation in cathode materials for non-lithium ion batteries: progress and challenges, Mater. Today 45 (2021) 169–190, https://doi.org/10.1016/j.mattod.2020.12.002.
[7] N. Yabuuchi, K. Kubota, M. Dahbi, S. Komaba, Research development on sodium-ion batteries, Chem. Rev. 114 (2014) 11636–11682, https://doi.org/10.1021/cr500192f.
[8] F. Xiong, Y. Jiang, L. Cheng, R. Yu, S. Tan, C. Tang, C. Zuo, Q. An, Y. Zhao, J.J. Gaumet, L. Mai, Low-strain TiP_2O_7 with three-dimensional ion channels as long-life and high-rate anode material for Mg-ion batteries, Interdiscip. Mater. 1 (2022) 140–147, https://doi.org/10.1002/idm2.12004.
[9] S. Tan, F. Xiong, J. Wang, Q. An, L. Mai, Crystal regulation towards rechargeable magnesium battery cathode materials, Mater. Horiz. 7 (2020) 1971–1995, https://doi.org/10.1039/d0mh00315h.
[10] C. Pei, F. Xiong, Y. Yin, Z. Liu, H. Tang, R. Sun, Q. An, L. Mai, Recent progress and challenges in the optimization of electrode materials for rechargeable magnesium batteries, Small 17 (2021), 2004108, https://doi.org/10.1002/smll.202004108.
[11] M.L. Mao, T. Gao, S.Y. Hou, C.S. Wang, A critical review of cathodes for rechargeable Mg batteries, Chem. Soc. Rev. 47 (2018) 8804–8841, https://doi.org/10.1039/c8cs00319j.
[12] F. Liu, T. Wang, X. Liu, L.Z. Fan, Challenges and recent progress on key materials for rechargeable magnesium batteries, Adv. Energy Mater. 11 (2021), 2000787, https://doi.org/10.1002/aenm.202000787.
[13] J. Tian, X. Zhou, Q. Wu, C. Li, Li-salt mediated Mg-rhodizonate batteries based on ultra-large cathode grains enabled by K-ion pillaring, Energy Storage Mater. 22 (2019) 218–227, https://doi.org/10.1016/j.ensm.2019.01.019.
[14] I. Shterenberg, M. Salama, Y. Gofer, E. Levi, D. Aurbach, The challenge of developing rechargeable magnesium batteries, MRS Bull. 39 (2014) 453–460, https://doi.org/10.1557/mrs.2014.61.
[15] J.W. Choi, D. Aurbach, Promise and reality of post-lithium-ion batteries with high energy densities, Nat. Rev. Mater. 1 (2016), 16013, https://doi.org/10.1038/natrevmats.2016.13.
[16] J. Muldoon, C.B. Bucur, T. Gregory, Quest for nonaqueous multivalent secondary batteries: magnesium and beyond, Chem. Rev. 114 (2014) 11683–11720, https://doi.org/10.1021/cr500049y.
[17] P. Canepa, G. Sai Gautam, D.C. Hannah, R. Malik, M. Liu, K.G. Gallagher, K.A. Persson, G. Ceder, Odyssey of multivalent cathode materials: open questions and future challenges, Chem. Rev. 117 (2017) 4287–4341, https://doi.org/10.1021/acs.chemrev.6b00614.
[18] D. Aurbach, Z. Lu, A. Schechter, Y. Gofer, H. Gizbar, R. Turgeman, Y. Cohen, M. Moshkovich, E. Levi, Prototype systems for rechargeable magnesium batteries, Nature 407 (2000) 724–727, https://doi.org/10.1038/35037553.
[19] F. Xiong, Y. Fan, S. Tan, L. Zhou, Y. Xu, C. Pei, Q. An, L. Mai, Magnesium storage performance and mechanism of CuS cathode, Nano Energy 47 (2018) 210–216, https://doi.org/10.1016/j.nanoen.2018.02.060.
[20] Y. Liang, H.D. Yoo, Y. Li, J. Shuai, H.A. Calderon, F.C. Robles Hernandez, L.C. Grabow, Y. Yao, Interlayer-expanded molybdenum disulfide nanocomposites for electrochemical magnesium storage, Nano Lett. 15 (2015) 2194–2202, https://doi.org/10.1021/acs.nanolett.5b00388.
[21] L. Zhou, F. Xiong, S. Tan, Q. An, Z. Wang, W. Yang, Z. Tao, Y. Yao, J. Chen, L. Mai, Nickel-iron bimetallic diselenides with enhanced kinetics for high-capacity and long-life magnesium batteries, Nano Energy 54 (2018) 360–366, https://doi.org/10.1016/j.nanoen.2018.10.033.
[22] B. Li, Z. Li, H. Chen, X. Zhang, S. Wu, H. Xu, Y. Yao, Y. Li, X. Li, Z. Hu, R.M. Laine, J. Zou, K. Zhang, Li+ additive accelerated structural transformation of MoS_2 cathodes for performance-enhancing rechargeable Mg^{2+} batteries, Mater. Today Energy 27 (2022), https://doi.org/10.1016/j.mtener.2022.101047.
[23] G. Gershinsky, H.D. Yoo, Y. Gofer, D. Aurbach, Electrochemical and spectroscopic analysis of Mg^{2+} intercalation into thin film electrodes of layered oxides: V_2O_5 and MoO_3, Langmuir 29 (2013) 10964–10972, https://doi.org/10.1021/la402391f.
[24] Q. An, Y. Li, H. Deog Yoo, S. Chen, Q. Ru, L. Mai, Y. Yao, Graphene decorated vanadium oxide nanowire aerogel for long-cycle-life magnesium battery cathodes, Nano Energy 18 (2015) 265–272, https://doi.org/10.1016/j.nanoen.2015.10.029.
[25] J. Yin, A.B. Brady, E.S. Takeuchi, A.C. Marschilok, K.J. Takeuchi, Magnesium-ion battery-relevant electrochemistry of $MgMn_2O_4$: crystallite size effects and the notable role of electrolyte water content, Chem. Commun. 53 (2017) 3665–3668, https://doi.org/10.1039/c7cc00265c.
[26] C. Dong, H. Kobayashi, I. Honma, Self-activation effect in bimetallic $MgMn_2O_4$ and boosting its electrochemical performance using metal-organic framework template for magnesium-ion battery cathodes, Mater. Today Energy 30 (2022), https://doi.org/10.1016/j.mtener.2022.101143.
[27] J. Wang, S. Tan, G. Zhang, Y. Jiang, Y. Yin, F. Xiong, Q. Li, D. Huang, Q. Zhang, L. Gu, Q. An, L. Mai, Fast and stable Mg^{2+} intercalation in a high voltage $NaV_2O_2(PO_4)_2F$/rGO cathode material for magnesium-ion batteries, Sci. China Mater. 63 (2020) 1651–1662, https://doi.org/10.1007/s40843-020-1311-1.
[28] L. Zhou, Q. Liu, Z. Zhang, K. Zhang, F. Xiong, S. Tan, Q. An, Y.M. Kang, Z. Zhou, L. Mai, Interlayer-spacing-regulated $VOPO_4$ nanosheets with fast kinetics for high-capacity and durable rechargeable magnesium batteries, Adv. Mater. 30 (2018), e1801984, https://doi.org/10.1002/adma.201801984.
[29] Y. Orikasa, T. Masese, Y. Koyama, T. Mori, M. Hattori, K. Yamamoto, T. Okado, Z.D. Huang, T. Minato, C. Tassel, J. Kim, Y. Kobayashi, T. Abe, H. Kageyama, Y. Uchimoto, High energy density rechargeable magnesium battery using earth-abundant and non-toxic elements, Sci. Rep. 4 (2014) 5622, https://doi.org/10.1038/srep05622.
[30] H. Dong, O. Tutusaus, Y. Liang, Y. Zhang, Z. Lebens-Higgins, W. Yang, R. Mohtadi, Y. Yao, High-power Mg batteries enabled by heterogeneous enolization redox chemistry and weakly coordinating electrolytes, Nat. Energy 5 (2020) 1043–1050, https://doi.org/10.1038/s41560-020-00734-0.
[31] H. Dong, Y. Liang, O. Tutusaus, R. Mohtadi, Y. Zhang, F. Hao, Y. Yao, Directing Mg-storage chemistry in organic polymers toward high-energy Mg batteries, Joule 3 (2019) 782–793, https://doi.org/10.1016/j.joule.2018.11.022.
[32] H. Tian, T. Gao, X. Li, X. Wang, C. Luo, X. Fan, C. Yang, L. Suo, Z. Ma, W. Han, C. Wang, High power rechargeable magnesium/iodine battery chemistry, Nat. Commun. 8 (2017), 14083, https://doi.org/10.1038/ncomms14083.
[33] H.S. Kim, T.S. Arthur, G.D. Allred, J. Zajicek, J.G. Newman, A.E. Rodnyansky, A.G. Oliver, W.C. Boggess, J. Muldoon, Structure and compatibility of a magnesium electrolyte with a sulphur cathode, Nat. Commun. 2 (2011) 427, https://doi.org/10.1038/ncomms1435.
[34] X. Xu, F. Xiong, J. Meng, X. Wang, C. Niu, Q. An, L. Mai, Vanadium-based nanomaterials: a promising family for emerging metal-ion batteries, Adv. Funct. Mater. 30 (2020), 1802564, https://doi.org/10.1002/adfm.201904398.
[35] H. Tang, Z. Peng, L. Wu, F. Xiong, C. Pei, Q. An, L. Mai, Vanadium-based cathode materials for rechargeable multivalent batteries: challenges and opportunities, Electrochem. Energy Rev. 1 (2018) 169–199, https://doi.org/10.1007/s41918-018-0007-y.
[36] J.P. Pereiraramos, R. Messina, J. Perichon, Electrochemical formation of a magnesium vanadium bronze $Mg_xV_2O_5$ in sulfone-based electrolytes at 150 °C, J. Electroanal. Chem. 218 (1987) 241–249, https://doi.org/10.1016/0022-0728(87)87019-5.
[37] W.-h. Yu, D.-z. Wang, B. Zhu, S.-j. Wang, L.-x. Xue, Insertion of bi-valence cations Mg^{2+} and Zn^{2+} into V_2O_5, Solid State Commun. 61 (1987) 271–273, https://doi.org/10.1016/0038-1098(87)90295-x.
[38] T.D. Gregory, R.J. Hoffman, R.C. Winterton, Nonaqueous electrochemistry of magnesium: applications to energy storage, J. Electrochem. Soc. 137 (1990) 775–780, https://doi.org/10.1149/1.2086553.
[39] P. Novák, W. Scheifele, F. Joho, O. Haas, Electrochemical insertion of magnesium into hydrated vanadium bronzes, J. Electrochem. Soc. 142 (1995) 2544–2550, https://doi.org/10.1149/1.2050051.
[40] L. Yu, X. Zhang, Electrochemical insertion of magnesium ions into V_2O_5 from aprotic electrolytes with varied water content, J. Colloid Interface Sci. 278 (2004) 160–165, https://doi.org/10.1016/j.jcis.2004.05.028.
[41] N. Sa, H. Wang, D.L. Proffit, A.L. Lipson, B. Key, M. Liu, Z. Feng, T.T. Fister, Y. Ren, C.-J. Sun, J.T. Vaughey, P.A. Fenter, K.A. Persson, A.K. Burrell, Is alpha-V_2O_5 a cathode material for Mg insertion batteries? J. Power Sources 323 (2016) 44–50, https://doi.org/10.1016/j.jpowsour.2016.05.028.
[42] M. Inamoto, H. Kurihara, T. Yajima, Vanadium pentoxide-based composite synthesized using microwave water plasma for cathode material in rechargeable magnesium batteries, Materials 6 (2013) 4514–4522, https://doi.org/10.3390/ma6104514.
[43] S.C. Lim, J. Lee, H.H. Kwak, J.W. Heo, M.S. Chae, D. Ahn, Y.H. Jang, H. Lee, S.T. Hong, Unraveling the magnesium-ion intercalation mechanism in vanadium pentoxide in a wet organic electrolyte by structural determination, Inorg. Chem. 56 (2017) 7668–7678, https://doi.org/10.1021/acs.inorgchem.7b00204.

[44] R. Verrelli, A.P. Black, C. Pattanathummasid, D.S. Tchitchekova, A. Ponrouch, J. Oró-Solé, C. Frontera, F. Bardé, P. Rozier, M.R. Palacín, On the strange case of divalent ions intercalation in V_2O_5, J. Power Sources 407 (2018) 162–172, https://doi.org/10.1016/j.jpowsour.2018.08.024.

[45] A. Mukherjee, N. Sa, P.J. Phillips, A. Burrell, J. Vaughey, R.F. Klie, Direct investigation of Mg intercalation into the orthorhombic V_2O_5 cathode using atomic-resolution transmission electron microscopy, Chem. Mater. 29 (2017) 2218–2226, https://doi.org/10.1021/acs.chemmater.6b05089.

[46] G. Sai Gautam, P. Canepa, A. Abdellahi, A. Urban, R. Malik, G. Ceder, The intercalation phase diagram of Mg in V_2O_5 from first-principles, Chem. Mater. 27 (2015) 3733–3742, https://doi.org/10.1021/acs.chemmater.5b00957.

[47] Q. Fu, A. Sarapulova, V. Trouillet, L. Zhu, F. Fauth, S. Mangold, E. Welter, S. Indris, M. Knapp, S. Dsoke, N. Bramnik, H. Ehrenberg, In operando synchrotron diffraction and in operando X-ray absorption spectroscopy investigations of orthorhombic V_2O_5 nanowires as cathode materials for Mg-ion batteries, J. Am. Chem. Soc. 141 (2019) 2305–2315, https://doi.org/10.1021/jacs.8b08998.

[48] R. Xiao, J. Xie, T. Luo, L. Huang, Y. Zhou, D. Yu, C. Chen, Y. Liu, Phase transformation and diffusion kinetics of V_2O_5 electrode in rechargeable Li and Mg batteries: a first-principle study, J. Phys. Chem. C 122 (2018) 1513–1521, https://doi.org/10.1021/acs.jpcc.7b11488.

[49] H.D. Yoo, J.R. Jokisaari, Y.-S. Yu, B.J. Kwon, L. Hu, S. Kim, S.-D. Han, M. Lopez, S.H. Lapidus, G.M. Nolis, B.J. Ingram, I. Bolotin, S. Ahmed, R.F. Klie, J.T. Vaughey, T.T. Fister, J. Cabana, Intercalation of magnesium into a layered vanadium oxide with high capacity, ACS Energy Lett. 4 (2019) 1528–1534, https://doi.org/10.1021/acsenergylett.9b00788.

[50] R. Attias, M. Salama, B. Hirsch, R. Pant, Y. Gofer, D. Aurbach, Anion effects on cathode electrochemical activity in rechargeable magnesium batteries: a case study of V_2O_5, ACS Energy Lett. 4 (2018) 209–214, https://doi.org/10.1021/acsenergylett.8b02140.

[51] R. Attias, M. Salama, B. Hirsch, Y. Gofer, D. Aurbach, Solvent effects on the reversible intercalation of magnesium-ions into V_2O_5 electrodes, Chemelectrochem 5 (2018) 3514–3524, https://doi.org/10.1002/celc.201800932.

[52] G.G. Amatucci, F. Badway, A. Singhal, B. Beaudoin, G. Skandan, T. Bowmer, I. Plitza, N. Pereira, T. Chapman, R. Jaworski, Investigation of yttrium and polyvalent ion intercalation into nanocrystalline vanadium oxide, J. Electrochem. Soc. 148 (2001) A940–A950, https://doi.org/10.1149/1.1383777.

[53] A. Mukherjee, S. Taragin, H. Aviv, I. Perelshtein, M. Noked, Rationally designed vanadium pentoxide as high capacity insertion material for Mg-ion, Adv. Funct. Mater. 30 (2020), https://doi.org/10.1002/adfm.202003518.

[54] Y. Xiao, M. Pan, J. Zou, R. Guo, X. Zeng, W. Ding, Surfactant induced formation of flower-like V_2O_5 microspheres as cathode materials for rechargeable magnesium batteries, Ionics 25 (2019) 5889–5897, https://doi.org/10.1007/s11581-019-03139-6.

[55] X. Du, G. Huang, Y. Qin, L. Wang, Solvothermal synthesis of GO/V_2O_5 composites as a cathode material for rechargeable magnesium batteries, RSC Adv. 5 (2015) 76352–76355, https://doi.org/10.1039/c5ra15284d.

[56] E. Sheha, M.H. Makled, W.M. Nouman, A. Bassyouni, S. Yaghmour, S. Abo-Elhassan, Vanadium oxide/graphene nanoplatelet as a cathode material for Mg-ion battery, Graphene 5 (2016) 178–188, https://doi.org/10.4236/graphene.2016.54015.

[57] I.D. Johnson, N. Stapleton, G. Nolis, D. Bauer, P. Parajuli, H.D. Yoo, L. Yin, B.J. Ingram, R.F. Klie, S. Lapidus, J.A. Darr, J. Cabana, Control of crystal size tailors the electrochemical performance of α-V_2O_5 as a Mg^{2+} intercalation host, Nanoscale 13 (2021) 10081–10091, https://doi.org/10.1039/d1nr03080a.

[58] D. Wu, Y. Zhuang, F. Wang, Y. Yang, J. Zeng, J. Zhao, High-rate performance magnesium batteries achieved by direct growth of honeycomb-like V_2O_5 electrodes with rich oxygen vacancies, Nano Res. (2021), https://doi.org/10.1007/s12274-021-3679-2.

[59] J. Yang, X. Wang, J. Wang, X. Dong, L. Zhu, D. Hou, W. Zeng, J. Wang, F. Pan, Ab initio investigations on metal ion pre-intercalation strategy of layered V_2O_5 cathode for magnesium-ion batteries, Appl. Surf. Sci. 569 (2021), 150983, https://doi.org/10.1016/j.apsusc.2021.150983.

[60] J.L. Andrews, A. Mukherjee, H.D. Yoo, A. Parija, P.M. Marley, S. Fakra, D. Prendergast, J. Cabana, R.F. Klie, S. Banerjee, Reversible Mg-ion insertion in a metastable one-dimensional polymorph of V_2O_5, Chem 4 (2018) 564–585, https://doi.org/10.1016/j.chempr.2017.12.018.

[61] Y. Zhang, L. Tao, C. Xie, D. Wang, Y. Zou, R. Chen, Y. Wang, C. Jia, S. Wang, Defect engineering on electrode materials for rechargeable batteries, Adv. Mater. 32 (2020), 1905923, https://doi.org/10.1002/adma.201905923.

[62] Z. Yao, Y. Yu, Q. Wu, M. Cui, X. Zhou, J. Liu, C. Li, Maximizing magnesiation capacity of nanowire cluster oxides by conductive macromolecule pillaring and multication intercalation, Small 17 (2021), 2102168, https://doi.org/10.1002/smll.202102168.

[63] G.S. Gautam, P. Canepa, R. Malik, M. Liu, K. Persson, G. Ceder, First-principles evaluation of multi-valent cation insertion into orthorhombic V_2O_5, Chem. Commun. 51 (2015) 13619–13622, https://doi.org/10.1039/c5cc04947d.

[64] Vadym V. Kulish, S. Manzhos, Comparison of Li, Na, Mg and Al-ion insertion in vanadium pentoxides and vanadium dioxides, RSC Adv. 7 (2017) 18643–18649, https://doi.org/10.1039/c7ra02474f.

[65] R. Trocoli, P. Parajuli, C. Frontera, A.P. Black, G.C.B. Alexander, I. Roy, M.E. Arroyo-de Dompablo, R.F. Klie, J. Cabana, M.R. Palacin, β-V_2O_5 as magnesium intercalation cathode, ACS Appl. Energy Mater. 5 (2022) 11964–11969, https://doi.org/10.1021/acsaem.2c02371.

[66] A. Parija, Y. Liang, J.L. Andrews, L.R. De Jesus, D. Prendergast, S. Banerjee, Topochemically de-intercalated phases of V_2O_5 as cathode materials for multivalent intercalation batteries: a first-principles evaluation, Chem. Mater. 28 (2016) 5611–5620, https://doi.org/10.1021/acs.chemmater.6b01006.

[67] P.M. Marley, T.A. Abtew, K.E. Farley, G.A. Horrocks, R.V. Dennis, P. Zhang, S. Banerjee, Emptying and filling a tunnel bronze, Chem. Sci. 6 (2015) 1712–1718, https://doi.org/10.1039/c4sc03748k.

[68] I.D. Johnson, G. Nolis, L. Yin, H.D. Yoo, P. Parajuli, A. Mukherjee, J.L. Andrews, M. Lopez, R.F. Klie, S. Banerjee, B.J. Ingram, S. Lapidus, J. Cabana, J.A. Darr, Enhanced charge storage of nanometric ζ-V_2O_5 in Mg electrolytes, Nanoscale 12 (2020) 22150–22160, https://doi.org/10.1039/d0nr05060a.

[69] Y. Cheng, Y. Shao, V. Raju, X. Ji, B.L. Mehdi, K.S. Han, M.H. Engelhard, G. Li, N.D. Browning, K.T. Mueller, J. Liu, Molecular storage of Mg ions with vanadium oxide nanoclusters, Adv. Funct. Mater. 26 (2016) 3446–3453, https://doi.org/10.1002/adfm.201505501.

[70] D. Kim, J.H. Ryu, Amorphous V_2O_5 positive electrode materials by precipitation method in magnesium rechargeable batteries, Electron. Mater. Lett. 15 (2019) 415–420, https://doi.org/10.1007/s13391-019-00138-7.

[71] H.K. Henry, B. Johnston, D. Liau, E. Sahadeo, S.B. Lee, Dual effect of structure and hydration on magnesium-ion insertion into electrodeposited V_2O_5 thin films, J. Electrochem. Soc. 167 (2020), 110523, https://doi.org/10.1149/1945-7111/aba36e.

[72] D.B. Le, S. Passerini, F. Coustier, J. Guo, T. Soderstrom, B.B. Owens, W.H. Smyrl, Intercalation of polyvalent cations into V_2O_5 aerogels, Chem. Mater. 10 (1998) 682, https://doi.org/10.1021/cm9705101.

[73] D. Imamura, M. Miyayama, M. Hibino, T. Kudo, Mg intercalation properties into V_2O_5 gel carbon composites under high-rate condition, J. Electrochem. Soc. 150 (2003) A753–A758, https://doi.org/10.1149/1.1571531.

[74] D. Imamura, Characterization of magnesium-intercalated V_2O_5/carbon composites, Solid State Ionics 161 (2003) 173–180, https://doi.org/10.1016/s0167-2738(03)00267-4.

[75] E. Levi, Y. Gofer, D. Aurbach, On the way to rechargeable Mg batteries: the challenge of new cathode materials, Chem. Mater. 22 (2010) 860–868, https://doi.org/10.1021/cm9016497.

[76] R.C. Massé, E. Uchaker, G. Cao, Beyond Li-ion: electrode materials for sodium- and magnesium-ion batteries, Sci. China Mater. 58 (2015) 715–766, https://doi.org/10.1007/s40843-015-0084-8.

[77] M. Inamoto, H. Kurihara, T. Yajima, Electrode performance of vanadium pentoxide xerogel prepared by microwave irradiation as an active cathode material for rechargeable magnesium batteries, Electrochemistry 80 (2012) 421–422, https://doi.org/10.5796/electrochemistry.80.421.

[78] M. Inamoto, H. Kurihara, T. Yajima, Electrode performance of sulfur-doped vanadium pentoxide gel prepared by microwave irradiation for rechargeable magnesium batteries, Curr. Phys. Chem. 4 (2014) 238–243, https://doi.org/10.2174/1877946805666150311234806.

[79] C. Zuo, Y. Xiao, X. Pan, F. Xiong, W. Zhang, J. Long, S. Dong, Q. An, P. Luo, Organic-inorganic superlattices of vanadium oxide@polyaniline for high-performance magnesium-ion batteries, ChemSusChem 14 (2021) 2093–2099, https://doi.org/10.1002/cssc.202100263.

[80] G. Sai Gautam, P. Canepa, W.D. Richards, R. Malik, G. Ceder, Role of structural H_2O in intercalation electrodes: the case of Mg in nanocrystalline xerogel-V_2O_5, Nano Lett. 16 (2016) 2426–2431, https://doi.org/10.1021/acs.nanolett.5b05273.

[81] S.D. Perera, R.B. Archer, C.A. Damin, R. Mendoza-Cruz, C.P. Rhodes, Controlling interlayer interactions in vanadium pentoxide-poly(ethylene oxide) nanocomposites for enhanced magnesium-ion charge transport and storage, J. Power Sources 343 (2017) 580–591, https://doi.org/10.1016/j.jpowsour.2017.01.052.

[82] J. Yang, X. Miao, C. Zhang, J. Zheng, C. Sun, Y. Zhang, H. Geng, In-situ lattice tunnel intercalation of vanadium pentoxide for improving long-term performance of rechargeable magnesium batteries, ChemNanoMat 8 (2022), https://doi.org/10.1002/cnma.202200025.

[83] H. Tang, N. Xu, C. Pei, F. Xiong, S. Tan, W. Luo, Q. An, L. Mai, $H_2V_3O_8$ nanowires as high-capacity cathode materials for magnesium-based battery, ACS Appl. Mater. Interfaces 9 (2017) 28667–28673, https://doi.org/10.1021/acsami.7b09924.

[84] C. Pei, F. Xiong, J. Sheng, Y. Yin, S. Tan, D. Wang, C. Han, Q. An, L. Mai, VO_2 nanoflakes as the cathode material of hybrid magnesium-lithium-ion batteries with high energy density, ACS Appl. Mater. Interfaces 9 (2017) 17060–17066, https://doi.org/10.1021/acsami.7b02480.

[85] M. Li, C. Pei, F. Xiong, S. Tan, Y. Yin, H. Tang, D. Huang, Q. An, L. Mai, A high energy density hybrid magnesium–lithium ion battery based on LiV_3O_8@GO cathode, Electrochim. Acta 320 (2019), 134556, https://doi.org/10.1016/j.electacta.2019.134556.

[86] W. Kou, J. Wu, Q. Zhang, Y. Shen, R. Bi, Y. Li, X. Miao, T. Yang, G. Yang, A VO_2/graphene oxide composite as a cathode material with high rate performance for hybrid Mg-Li batteries, J. Alloys Compd. 924 (2022), 166414, https://doi.org/10.1016/j.jallcom.2022.166414.

[87] Y.J. Li, Y.J. Zheng, K. Guo, J.T. Zhao, C.L. Li, Mg-Li hybrid batteries: the combination of fast kinetics and reduced overpotential, Energy Mater Adv 2022 (2022), 9840837, https://doi.org/10.34133/2022/9840837.

[88] S. Tepavcevic, Y. Liu, D. Zhou, B. Lai, J. Maser, X. Zuo, H. Chan, P. Kral, C.S. Johnson, V. Stamenkovic, N.M. Markovic, T. Rajh, Nanostructured layered

cathode for rechargeable Mg-ion batteries, ACS Nano 9 (2015) 8194–8205, https://doi.org/10.1021/acsnano.5b02450.
[89] T. Luo, Y. Liu, H. Su, R. Xiao, L. Huang, Q. Xiang, Y. Zhou, C. Chen, Nano-structured-VO_2(B): a high-capacity magnesium-ion cathode and its electrochemical reaction mechanism, Electrochim. Acta 260 (2018) 805–813, https://doi.org/10.1016/j.electacta.2017.12.042.
[90] M. Rastgoo-Deylami, M.S. Chae, S.-T. Hong, $H_2V_3O_8$ as a high energy cathode material for nonaqueous magnesium-ion batteries, Chem. Mater. 30 (2018) 7464–7472, https://doi.org/10.1021/acs.chemmater.8b01381.
[91] P.G. Bruce, F. Krok, J. Nowinski, V.C. Gibson, K. Tavakkoli, Chemical intercalation of magnesium into solid hosts, J. Mater. Chem. 1 (1991) 705–706, https://doi.org/10.1039/jm9910100705.
[92] Z. Wang, Y. Zhang, S. Xiao, H. Zhai, Y. Zhu, C. Cao, Microwave-assisted synthesis of metallic V_6O_{13} nanosheet as high-capacity cathode for magnesium storage, Mater. Lett. 308 (2022), 131279, https://doi.org/10.1016/j.matlet.2021.131279.
[93] C. Pei, M. Jin, Y. Yin, F. Xiong, Y. Jiang, X. Yuan, F. Wang, Q. An, Intercalation-type V_2O_3 with fast Mg^{2+} diffusion kinetics for high-capacity and long-life Mg-ion storage, ACS Sustain. Chem. Eng. 8 (2020) 16164–16171, https://doi.org/10.1021/acssuschemeng.0c04734.
[94] L. Jiao, H. Yuan, Y. Wang, J. Cao, Y. Wang, Mg intercalation properties into open-ended vanadium oxide nanotubes, Electrochem. Commun. 7 (2005) 431–436, https://doi.org/10.1016/j.elecom.2005.02.017.
[95] L. Jiao, H. Yuan, Y. Si, Y. Wang, J. Cao, X. Gao, M. Zhao, X. Zhou, Y. Wang, Electrochemical insertion of magnesium in open-ended vanadium oxide nanotubes, J. Power Sources 156 (2006) 673–676, https://doi.org/10.1016/j.jpowsour.2005.06.004.
[96] L.-F. Jiao, H.-T. Yuan, Y.-C. Si, Y.-J. Wang, Y.-M. Wang, Synthesis of $Cu_{0.1}$-doped vanadium oxide nanotubes and their application as cathode materials for rechargeable magnesium batteries, Electrochem. Commun. 8 (2006) 1041–1044, https://doi.org/10.1016/j.elecom.2006.03.043.
[97] R.-H. Kim, J.-S. Kim, H.-J. Kim, W.-S. Chang, D.-W. Han, S.-S. Lee, S.-G. Doo, Highly reduced VO_x nanotube cathode materials with ultra-high capacity for magnesium ion batteries, J. Mater. Chem. 2 (2014) 20636–20641, https://doi.org/10.1039/c4ta05564k.
[98] C.K. Christensen, E.D. Bøjesen, D.R. Sørensen, J.H. Kristensen, J.K. Mathiesen, B.B. Iversen, D.B. Ravnsbæk, Structural evolution during lithium- and magnesium-ion intercalation in vanadium oxide nanotube electrodes for battery applications, ACS Appl. Nano Mater. 1 (2018) 5071–5082, https://doi.org/10.1021/acsanm.8b01183.
[99] P. Novák, W. Scheifele, O. Haas, Magnesium insertion batteries — an alternative to lithium? J. Power Sources 54 (1995) 479–482, https://doi.org/10.1016/0378-7753(94)02129-q.
[100] M. Rashad, H. Zhang, M. Asif, K. Feng, X. Li, H. Zhang, Low-cost room-temperature synthesis of NaV_3O_8.1.69H_2O nanobelts for Mg batteries, ACS Appl. Mater. Interfaces 10 (2018) 4757–4766, https://doi.org/10.1021/acsami.7b18682.
[101] R. Sun, X. Ji, C. Luo, S. Hou, P. Hu, X. Pu, L. Cao, L. Mai, C. Wang, Water-pillared sodium vanadium bronze nanowires for enhanced rechargeable magnesium ion storage, Small 16 (2020), 2000741, https://doi.org/10.1002/smll.202000741.
[102] X. Wang, X. Zhang, G. Zhao, H. Hong, Z. Tang, X. Xu, H. Li, C. Zhi, C. Han, Ether-water hybrid electrolyte contributing to excellent Mg ion storage in layered sodium vanadate, ACS Nano (2022), https://doi.org/10.1021/acsnano.1c11590.
[103] H. Tang, F. Xiong, Y. Jiang, C. Pei, S. Tan, W. Yang, M. Li, Q. An, L. Mai, Alkali ions pre-intercalated layered vanadium oxide nanowires for stable magnesium ions storage, Nano Energy 58 (2019) 347–354, https://doi.org/10.1016/j.nanoen.2019.01.053.
[104] M. Cabello, F. Nacimiento, R. Alcántara, P. Lavela, G. Ortiz, J.L. Tirado, Nanobelts of beta-sodium vanadate as electrode for magnesium and dual magnesium-sodium batteries, J. Electrochem. Soc. 163 (2016) A2781–A2790, https://doi.org/10.1149/2.1211613jes.
[105] D. Wu, J. Zeng, H. Hua, J. Wu, Y. Yang, J. Zhao, NaV_6O_{15}: a promising cathode material for insertion/extraction of Mg^{2+} with excellent cycling performance, Nano Res. 13 (2020) 335–343, https://doi.org/10.1007/s12274-019-2602-6.
[106] D.C. Hannah, G. Sai Gautam, P. Canepa, Z. Rong, G. Ceder, Magnesium ion mobility in post-spinels accessible at ambient pressure, Chem. Commun. 53 (2017) 5171–5174, https://doi.org/10.1039/c7cc01092c.
[107] X. Sun, L. Blanc, G.M. Nolis, P. Bonnick, J. Cabana, L.F. Nazar, $NaV_{1.25}Ti_{0.75}O_4$: a potential post-spinel cathode material for Mg batteries, Chem. Mater. 30 (2018) 121–128, https://doi.org/10.1021/acs.chemmater.7b03383.
[108] S.H. Lee, R.A. DiLeo, A.C. Marschilok, K.J. Takeuchi, E.S. Takeuchi, Sol gel based synthesis and electrochemistry of magnesium vanadium oxide: a promising cathode material for secondary magnesium ion batteries, ECS Electrochem. Lett. 3 (2014) A87–A90, https://doi.org/10.1149/2.0021408eel.
[109] J. Yin, C.J. Pelliccione, S.H. Lee, E.S. Takeuchi, K.J. Takeuchi, A.C. Marschilok, Communication—sol-gel synthesized magnesium vanadium oxide, $Mg_xV_2O_5 \cdot nH_2O$: the role of structural Mg^{2+} on battery performance, J. Electrochem. Soc. 163 (2016) A1941–A1943, https://doi.org/10.1149/2.0781609jes.
[110] Y. Xu, X. Deng, Q. Li, G. Zhang, F. Xiong, S. Tan, Q. Wei, J. Lu, J. Li, Q. An, L. Mai, Vanadium oxide pillared by interlayer Mg^{2+} ions and water as ultralong-life cathodes for magnesium-ion batteries, Chem 5 (2019) 1194–1209, https://doi.org/10.1016/j.chempr.2019.02.014.
[111] N. Kuganathan, K. Davazoglou, A. Chroneos, Computer modeling investigation of MgV_2O_4 for Mg-ion batteries, J. Appl. Phys. 127 (2020), https://doi.org/10.1063/1.5139114.
[112] L. Hu, J.R. Jokisaari, B.J. Kwon, L. Yin, S. Kim, H. Park, S.H. Lapidus, R.F. Klie, B. Key, P. Zapol, B.J. Ingram, J.T. Vaughey, J. Cabana, High capacity for Mg^{2+} deintercalation in spinel vanadium oxide nanocrystals, ACS Energy Lett. 5 (2020) 2721–2727, https://doi.org/10.1021/acsenergylett.0c01189.
[113] C. Zuo, W. Tang, B. Lan, F. Xiong, H. Tang, S. Dong, W. Zhang, C. Tang, J. Li, Y. Ruan, S. Xi, Q. An, P. Luo, Unexpected discovery of magnesium-vanadium spinel oxide containing extractable Mg^{2+} as a high-capacity cathode material for magnesium ion batteries, Chem. Eng. J. 405 (2021), 127005, https://doi.org/10.1016/j.cej.2020.127005.
[114] M. Liu, Z. Rong, R. Malik, P. Canepa, A. Jain, G. Ceder, K.A. Persson, Spinel compounds as multivalent battery cathodes: a systematic evaluation based on ab initio calculations, Energy Environ. Sci. 8 (2015) 964–974, https://doi.org/10.1039/c4ee03389b.
[115] Y. Idemoto, N. Kawakami, N. Ishida, N. Kitamura, Synthesis, electrochemical properties and changes of crystal and electronic structures in charge/discharge process of spinel type cathode-materials $Mg(Mg_{0.5}V_{1.5-x}Ni_x)O_4$ (x = 0, 0.1, 0.2, 0.3) for magnesium secondary batteries, Electrochemistry 87 (2019) 281–288, https://doi.org/10.5796/electrochemistry.19-00031.
[116] W. Kaveevivitchai, A.J. Jacobson, High capacity rechargeable magnesium-ion batteries based on a microporous molybdenum–vanadium oxide cathode, Chem. Mater. 28 (2016) 4593–4601, https://doi.org/10.1021/acs.chemmater.6b01245.
[117] X. Miao, Z. Chen, N. Wang, Y. Nuli, J. Wang, J. Yang, S.-i. Hirano, Electrospun V_2MoO_8 as a cathode material for rechargeable batteries with Mg metal anode, Nano Energy 34 (2017) 26–35, https://doi.org/10.1016/j.nanoen.2017.02.014.
[118] C. Tang, F. Xiong, B. Lan, S. Tan, S. Dong, W. Zhang, C. Zuo, W. Tang, Q. An, P. Luo, Constructing a disorder/order structure for enhanced magnesium storage, Chem. Eng. J. 382 (2020), 123049, https://doi.org/10.1016/j.cej.2019.123049.
[119] H. Tang, C. Zuo, F. Xiong, C. Pei, S. Tan, P. Luo, W. Yang, Q. An, L. Mai, Flexible three-dimensional-networked iron vanadate nanosheet arrays/carbon cloths as high-performance cathodes for magnesium ion batteries, Sci. China Mater. 65 (2022) 2197–2206, https://doi.org/10.1007/s40843-021-2000-y.
[120] X. Deng, Y. Xu, Q. An, F. Xiong, S. Tan, L. Wu, L. Mai, Manganese ion pre-intercalated hydrated vanadium oxide as a high-performance cathode for magnesium ion batteries, J. Mater. Chem. 7 (2019) 10644–10650, https://doi.org/10.1039/c8ta11236c.
[121] E.A. Esparcia, M.S. Chae, J.D. Ocon, S.-T. Hong, Ammonium vanadium bronze $(NH_4V_4O_{10})$ as a high-capacity cathode material for nonaqueous magnesium-ion batteries, Chem. Mater. 30 (2018) 3690–3696, https://doi.org/10.1021/acs.chemmater.8b00462.
[122] L. Wei, R. Lian, D. Wang, Y. Zhao, D. Yang, H. Zhao, Y. Wang, G. Chen, Y. Wei, Magnesium ion storage properties in a layered $(NH_4)_2V_6O_{16} \cdot 1.5H_2O$ nanobelt cathode material activated by lattice water, ACS Appl. Mater. Interfaces 13 (2021) 30625–30632, https://doi.org/10.1021/acsami.1c06398.
[123] H. Tang, F. Chao, H. Chen, R. Jia, H. Luo, F. Xiong, X. Yao, W. Zhang, C. Zuo, J. Wang, P. Luo, Q. An, Water-lubricated aluminum vanadate for enhanced rechargeable magnesium ion storage, Small 18 (2022), 2203525, https://doi.org/10.1002/smll.202203525.
[124] M. Mao, X. Ji, S. Hou, T. Gao, F. Wang, L. Chen, X. Fan, J. Chen, J. Ma, C. Wang, Tuning anionic chemistry to improve kinetics of Mg intercalation, Chem. Mater. 31 (2019) 3183–3191, https://doi.org/10.1021/acs.chemmater.8b05218.
[125] X. Xue, R. Chen, C. Yan, P. Zhao, Y. Hu, W. Kong, H. Lin, L. Wang, Z. Jin, One-step synthesis of 2-ethylhexylamine pillared vanadium disulfide nanoflowers with ultralarge interlayer spacing for high-performance magnesium storage, Adv. Energy Mater. 9 (2019), 1900145, https://doi.org/10.1002/aenm.201900145.
[126] P. Jing, H. Lu, W. Yang, Y. Cao, Interlayer-expanded and binder-free VS_2 nanosheets assemblies for enhanced Mg^{2+} and Li^+/Mg^{2+} hybrid ion storage, Electrochim. Acta 330 (2020), 135263, https://doi.org/10.1016/j.electacta.2019.135263.
[127] R. Sun, C. Pei, J. Sheng, D. Wang, L. Wu, S. Liu, Q. An, L. Mai, High-rate and long-life VS_2 cathodes for hybrid magnesium-based battery, Energy Storage Mater. 12 (2018) 61–68, https://doi.org/10.1016/j.ensm.2017.11.012.
[128] Y. Zhao, D. Wang, D. Yang, L. Wei, B. Liu, X. Wang, G. Chen, Y. Wei, Superior Mg^{2+} storage properties of VS_2 nanosheets by using an APC-$PP_{14}Cl$/THF electrolyte, Energy Storage Mater. 23 (2019) 749–756, https://doi.org/10.1016/j.ensm.2019.04.004.
[129] Y. Gu, Y. Katsura, T. Yoshino, H. Takagi, K. Taniguchi, Rechargeable magnesium-ion battery based on a $TiSe_2$-cathode with d-p orbital hybridized electronic structure, Sci. Rep. 5 (2015), 12486, https://doi.org/10.1038/srep12486.
[130] D. Tao, F. Xu, VSe_2 nanosheets constructing hierarchical rods cathode for rechargeable magnesium batteries, Mater. Lett. 300 (2021), 130221, https://doi.org/10.1016/j.matlet.2021.130221.
[131] Y.-p. Gao, Z. Zhai, Y. Dong, Y. Pang, J. Chen, G. Li, 1 T-VSe_2 nanoparticles cooperated with reduced graphene oxide as a superior cathode material for rechargeable Mg-ion batteries, Appl. Surf. Sci. 592 (2022), 153141, https://doi.org/10.1016/j.apsusc.2022.153141.

[132] Y. Wang, Z. Liu, C. Wang, X. Yi, R. Chen, L. Ma, Y. Hu, G. Zhu, T. Chen, Z. Tie, J. Ma, J. Liu, Z. Jin, Highly branched VS_4 nanodendrites with 1D atomic-chain structure as a promising cathode material for long-cycling magnesium batteries, Adv. Mater. 30 (2018), 1802563, https://doi.org/10.1002/adma.201802563.
[133] Z. Li, B.P. Vinayan, P. Jankowski, C. Njel, A. Roy, T. Vegge, J. Maibach, J.M.G. Lastra, M. Fichtner, Z. Zhao-Karger, Multi-electron reactions enabled by anion-based redox chemistry for high-energy multivalent rechargeable batteries, Angew. Chem. Int. Ed. 59 (2020) 11483–11490, https://doi.org/10.1002/anie.202002560.
[134] S. Dey, J. Lee, S. Britto, J.M. Stratford, E.N. Keyzer, M.T. Dunstan, G. Cibin, S.J. Cassidy, M. Elgaml, C.P. Grey, Exploring cation-anion redox processes in one-dimensional linear chain vanadium tetrasulfide rechargeable magnesium ion cathodes, J. Am. Chem. Soc. 142 (2020) 19588–19601, https://doi.org/10.1021/jacs.0c08222.
[135] J. Zhu, X. Zhang, H. Gao, Y. Shao, Y. Liu, Y. Zhu, J. Zhang, L. Li, VS_4 anchored on Ti_3C_2 MXene as a high-performance cathode material for magnesium ion battery, J. Power Sources 518 (2022), 230731, https://doi.org/10.1016/j.jpowsour.2021.230731.
[136] J. Li, Y. Xu, Y. He, Z. Zhang, C. Zhu, X. Zhou, Core-shell-structured carbon nanotube@VS_4 nanonecklaces as a high-performance cathode material for magnesium-ion batteries, J. Phys. Chem. Lett. 13 (2022) 5726–5733, https://doi.org/10.1021/acs.jpclett.2c01299.
[137] S. Ding, Z. Li, X. Dai, C. Sun, A. Meng, Mo-doped VS_4 with interlayer-expanded and engineering sulfur vacancies as cathode for advanced magnesium storage, Chem. Eng. J. 417 (2021), 129328, https://doi.org/10.1016/j.cej.2021.129328.
[138] S. Ding, X. Dai, Z. Li, A. Meng, L. Wang, G. Li, S. Li, Strategy of cation/anion co-doping for potential elevating of VS_4 cathode for magnesium ion batteries, Chem. Eng. J. 439 (2022), https://doi.org/10.1016/j.cej.2022.135778.
[139] S. Ding, X. Dai, Y. Tian, G. Song, Z. Li, A. Meng, L. Wang, G. Li, W. Wang, J. Huang, S. Li, Synergy strategy of electrical conductivity enhancement and vacancy introduction for improving the performance of VS_4 magnesium-ion battery cathode, ACS Appl. Mater. Interfaces 13 (2021) 54005–54017, https://doi.org/10.1021/acsami.1c17023.
[140] C. Pei, Y. Yin, R. Sun, F. Xiong, X. Liao, H. Tang, S. Tan, Y. Zhao, Q. An, L. Mai, Interchain-expanded vanadium tetrasulfide with fast kinetics for rechargeable magnesium batteries, ACS Appl. Mater. Interfaces 11 (2019) 31954–31961, https://doi.org/10.1021/acsami.9b09592.
[141] S. Ding, X. Dai, Y. Tian, B. Song, L. Wang, G. Li, S. Li, J. Huang, Z. Li, A. Meng, Insight into the coordinating mechanism of multi-electron reaction and structural stability induced by K^+ pre-intercalation for magnesium ions batteries, Nano Energy 93 (2022), https://doi.org/10.1016/j.nanoen.2021.106838.
[142] S.Q. Ding, X. Dai, Z.J. Li, C.S. Wang, A. Meng, L. Wang, G.C. Li, J.F. Huang, S.X. Li, PVP-induced synergistic engineering of interlayer, self-doping, active surface and vacancies in VS_4 for enhancing magnesium ions storage and durability, Energy Storage Mater. 47 (2022) 211–222, https://doi.org/10.1016/j.ensm.2022.02.023.
[143] Z.-D. Huang, T. Masese, Y. Orikasa, T. Mori, k. Yamamoto, Vanadium phosphate as a promising high-voltage magnesium ion (de)-intercalation cathode host, RSC Adv. 5 (2015) 8598–8603, https://doi.org/10.1039/c4ra14416c.
[144] C. Li, W. Wu, Y. Liu, X. Yang, Z. Qin, Z. Jia, X. Sun, Facilitating Mg^{2+} diffusion in high potential $Li_xV_2(PO_4)_3$ cathode material with a co-insertion strategy for rechargeable Mg-ion batteries, J. Power Sources 520 (2022), 230853, https://doi.org/10.1016/j.jpowsour.2021.230853.
[145] F. Wang, X. Fan, T. Gao, W. Sun, Z. Ma, C. Yang, F. Han, K. Xu, C. Wang, High-voltage aqueous magnesium ion batteries, ACS Cent. Sci. 3 (2017) 1121–1128, https://doi.org/10.1021/acscentsci.7b00361.
[146] M. Rashad, H. Zhang, X. Li, H. Zhang, Fast kinetics of Mg^{2+}/Li^+ hybrid ions in a polyanion $Li_3V_2(PO_4)_3$ cathode in a wide temperature range, J. Mater. Chem. 7 (2019) 9968–9976, https://doi.org/10.1039/c9ta00502a.
[147] G. Hasegawa, Y. Akiyama, M. Tanaka, R. Ishikawa, H. Akamatsu, Y. Ikuhara, K. Hayashi, Reversible electrochemical insertion/extraction of magnesium ion into/from robust NASICON-type crystal lattice in a $Mg(BF_4)_2$-based electrolyte, ACS Appl. Energy Mater. 3 (2020) 6824–6833, https://doi.org/10.1021/acsaem.0c00943.
[148] M. Cabello, R. Alcántara, F. Nacimiento, P. Lavela, M.J. Aragón, J.L. Tirado, $Na_3V_2(PO_4)_3$ as electrode material for rechargeable magnesium batteries: a case of sodium-magnesium hybrid battery, Electrochim. Acta 246 (2017) 908–913, https://doi.org/10.1016/j.electacta.2017.06.080.
[149] J. Zeng, Y. Yang, S. Lai, J. Huang, Y. Zhang, J. Wang, J. Zhao, A promising high-voltage cathode material based on mesoporous $Na_3V_2(PO_4)_3$/C for rechargeable magnesium batteries, Chem. Eur J. 23 (2017) 16898–16905, https://doi.org/10.1002/chem.201704303.
[150] J. Zeng, D. Wu, X. Wang, J. Wu, J. Li, J. Wang, J. Zhao, Insights into the Mg storage property and mechanism based on the honeycomb-like structured $Na_3V_2(PO_4)_3$/C/G in anhydrous electrolyte, Chem. Eng. J. 372 (2019) 37–45, https://doi.org/10.1016/j.cej.2019.04.128.
[151] D.S. Tchitchekova, D. Monti, P. Johansson, F. Bardé, A. Randon-Vitanova, M.R. Palacín, A. Ponrouch, On the reliability of half-cell tests for monovalent (Li^+, Na^+) and divalent (Mg^{2+}, Ca^{2+}) cation based batteries, J. Electrochem. Soc. 164 (2017) A1384–A1392, https://doi.org/10.1149/2.0411707jes.
[152] M.J. Aragón, P. Lavela, P. Recio, R. Alcántara, J.L. Tirado, On the influence of particle morphology to provide high performing chemically desodiated C@$NaV_2(PO_4)_3$ as cathode for rechargeable magnesium batteries, J. Electroanal. Chem. 827 (2018) 128–136, https://doi.org/10.1016/j.jelechem.2018.09.013.
[153] Y. Li, Q. An, Y. Cheng, Y. Liang, Y. Ren, C.-J. Sun, H. Dong, Z. Tang, G. Li, Y. Yao, A high-voltage rechargeable magnesium-sodium hybrid battery, Nano Energy 34 (2017) 188–194, https://doi.org/10.1016/j.nanoen.2017.02.012.
[154] D. Zhao, S. Chen, Y. Lai, M. Ding, Y. Cao, Z. Chen, A stable "rocking-chair" zinc-ion battery boosted by low-strain $Zn_3V_4(PO_4)_6$ cathode, Nano Energy 100 (2022), 107520, https://doi.org/10.1016/j.nanoen.2022.107520.
[155] X. Ji, J. Chen, F. Wang, W. Sun, Y. Ruan, L. Miao, J. Jiang, C. Wang, Water-activated $VOPO_4$ for magnesium ion batteries, Nano Lett. 18 (2018) 6441–6448, https://doi.org/10.1021/acs.nanolett.8b02854.
[156] S. Rubio, Z. Liang, X. Liu, P. Lavela, J.L. Tirado, R. Stoyanova, E. Zhecheva, R. Liu, W. Zuo, Y. Yang, C. Pérez-Vicente, G.F. Ortiz, Reversible multi-electron storage enabled by $Na_5V(PO_4)_2F_2$ for rechargeable magnesium batteries, Energy Storage Mater. 38 (2021) 462–472, https://doi.org/10.1016/j.ensm.2021.03.035.
[157] C. Li, L. Lin, W. Wu, X. Sun, A high potential polyanion cathode material for rechargeable Mg-ion batteries, Small Methods 6 (2022), 2200363, https://doi.org/10.1002/smtd.202200363.
[158] S. Dongmo, F. Maroni, C. Gauckler, M. Marinaro, M. Wohlfahrt-Mehrens, On the electrochemical insertion of Mg^{2+} in $Na_7V_4(P_2O_7)_4(PO_4)$ and $Na_3V_2(PO_4)_3$ host materials, J. Electrochem. Soc. 168 (2021), 120541, https://doi.org/10.1149/1945-7111/ac412b.
[159] N.K. Wally, E. Sheha, B.M. Kamal, A.E. Hannora, M.M. El-Desoky, Exploring the electrochemical properties of Na_2S-V_2O_5-P_2O_5 glass-ceramic nanocomposites as a cathode for magnesium-ion batteries, J. Alloys Compd. 895 (2022), 162644, https://doi.org/10.1016/j.jallcom.2021.162644.
[160] H.-t. Yuan, L.-f. Jiao, J.-s. Cao, X.-s. Liu, M. Zhao, Y.-m. Wang, Preparation and electrochemical magnesium insertion behaviors of MgV_2O_6, J Electrochemistry 10 (2004) 460–463.
[161] J.-Z. Sun, Study of MgV_2O_6 as cathode material for secondary magnesium batteries, Asian J. Chem. 23 (2011) 1399–1400.
[162] Z. Li, S. Ding, J. Yin, M. Zhang, C. Sun, A. Meng, Morphology-dependent electrochemical performance of VS_4 for rechargeable magnesium battery and its magnesiation/demagnesiation mechanism, J. Power Sources 451 (2020), https://doi.org/10.1016/j.jpowsour.2020.227815.
[163] T.S. Arthur, K. Kato, J. Germain, J. Guo, P.A. Glans, Y.S. Liu, D. Holmes, X. Fan, F. Mizuno, Amorphous V_2O_5-P_2O_5 as high-voltage cathodes for magnesium batteries, Chem. Commun. 51 (2015) 15657–15660, https://doi.org/10.1039/c5cc07161e.
[164] S. Rubio, R. Liu, X. Liu, P. Lavela, J.L. Tirado, Q. Li, Z. Liang, G.F. Ortiz, Y. Yang, Exploring the high-voltage Mg^{2+}/Na^+ co-intercalation reaction of $Na_3VCr(PO_4)_3$ in Mg-ion batteries, J. Mater. Chem. 7 (2019) 18081–18091, https://doi.org/10.1039/c9ta05608d.